2

Stochastic soil moisture dynamics and water balance

This chapter presents a probabilistic model for the temporal dynamics of soil moisture, with the goal of providing a simplified yet realistic description amenable to analytical solutions. Such an analysis is the necessary starting point for the quantitative understanding of the impacts of soil moisture on ecosystems' dynamics, such as the vegetation response to water stress, the hydrologic control on cycles of soil nutrients, and the dynamics of plant competition for water. The same approach may also be useful to obtain insights into other processes closely related to soil moisture dynamics, such as soil–atmosphere interactions, soil production, and soil gas emissions.

The probabilistic soil moisture model that we describe in this chapter was originally proposed by Rodríguez-Iturbe et al. (1999a) and improved by Laio et al. (2001a). Here all the various physical processes involved in the soil moisture dynamics, the simplifying assumptions, and their related implications are discussed in detail. Particular attention is devoted to the role of soil properties and plant transpiration characteristics.

The solution of the problem in probabilistic terms, which is made necessary by the introduction of the stochastic representation of rainfall, is carried out for statistically steady-state conditions during a growing season. The results allow assessment of the roles of climate, soil, and vegetation on the soil moisture probability density function (pdf) and on the average long-term water balance. The chapter closes with a brief discussion of possible simplifications of the soil moisture dynamics that are of interest when considering the large-scale water balance.

2.1 Soil water balance at a point

The soil water balance is the mass conservation of soil water as a function of time. In general, it is a very complex problem that depends on many

interactions and processes. We will consider the water balance vertically averaged over the root zone, focusing on the most important components as sketched in Figure 2.1.

The state variable regulating the water balance is the relative soil moisture, s, which represents the fraction of pore volume containing water. The total volume of soil is given by the sum of the volumes of air, water, and mineral components, i.e., $V_s = V_a + V_w + V_m$. The porosity is defined as

$$n = \frac{V_a + V_w}{V_s}, \tag{2.1}$$

and the volumetric water content, θ, is the ratio of water volume to soil volume, so that the relative soil moisture is

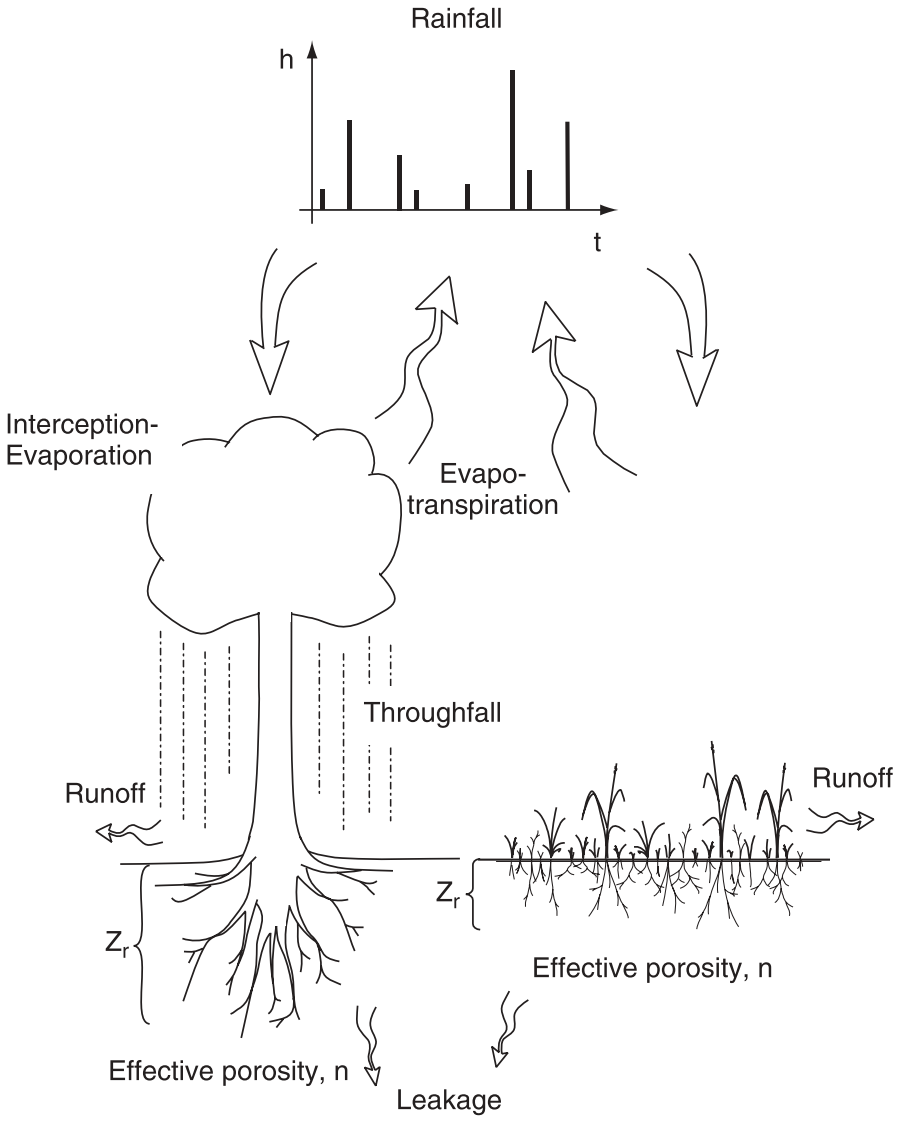

Figure 2.1 Schematic representation of the various mechanisms of the soil water balance with emphasis on the role of different functional vegetation types. After Laio et al. (2001a).

$$s = \frac{V_w}{V_a + V_w} = \frac{\theta}{n}, \tag{2.2}$$

$0 \leq s \leq 1$. Denoting the rooting depth by Z_r, snZ_r represents the volume of water contained in the root zone per unit area of ground.

With the above definitions and under the simplifying assumption that the lateral contributions can be neglected (i.e., negligible topographic effects over the area under consideration), the vertically averaged soil moisture balance at a point may be expressed as

$$nZ_r \frac{ds(t)}{dt} = \varphi[s(t), t] - \chi[s(t)], \tag{2.3}$$

where t is time, $\varphi[s(t), t]$ is the rate of infiltration from rainfall, and $\chi[s(t)]$ is the rate of soil moisture losses from the root zone. The terms on the r.h.s. of Eq. (2.3) represent water fluxes, i.e ., volumes of water per unit area of ground and per unit of time (e.g., mm day^{-1}).

The infiltration from rainfall, $\varphi[s(t), t]$, is the stochastic component of the balance. It represents the part of rainfall that actually reaches the soil column, i.e.,

$$\varphi[s(t), t] = R(t) - I(t) - Q[s(t), t], \tag{2.4}$$

where $R(t)$ is the rainfall rate, $I(t)$ is the amount of rainfall lost through canopy interception, and $Q[s(t), t]$ is the rate of runoff.

The water losses from the soil are from two different mechanisms

$$\chi[s(t)] = E[s(t)] + L[s(t)], \tag{2.5}$$

namely, $E[s(t)]$ and $L[s(t)]$, the rates of evapotranspiration and leakage, respectively.

Equation (2.3) is a stochastic, ordinary differential equation for the state variable $s(t)$. It is of fundamental hydrologic importance and underlies most of the dynamics studied in this book. For simplicity of notation, in what follows we will dispense with the indication of the time dependence of soil moisture whenever it is not necessary.

2.1.1 Rainfall modeling

At small spatial scales, where the contribution of local soil-moisture recycling to rainfall is negligible, the rainfall input can be treated as an external random forcing, independent of the soil moisture state. The inclusion of the stochastic nature of rainfall is essential when attempting proper modeling of soil moisture

dynamics, since the response of vegetation (i.e., resistance to drought, productivity, reproduction and germination, etc.) in water-controlled ecosystems is strongly linked to the intermittent and unpredictable character of rainfall availability (e.g., Noy-Meir, 1973).

Since both the occurrence and amount of rainfall can be considered to be stochastic, the occurrence of rainfall is idealized as a series of point events in continuous time, arising according to a Poisson process of rate λ and each carrying a random amount of rainfall extracted from a given distribution. The temporal structure within each rain event is ignored and the marked Poisson process representing precipitation is physically interpreted at a daily time scale, where the pulses of rainfall correspond to daily precipitation assumed to be concentrated at an instant in time.

With these assumptions, the distribution of the times τ between precipitation events is exponential with mean $1/\lambda$ (e.g., Cox and Miller, 1965), i.e.,

$$f_T(\tau) = \lambda e^{-\lambda\tau}, \text{ for } \tau \geq 0, \tag{2.6}$$

while the depth of rainfall events is assumed to be an independent random variable h, described by an exponential probability density function

$$f_H(h) = \frac{1}{\alpha} e^{-\frac{1}{\alpha}h}, \text{ for } h \geq 0, \tag{2.7}$$

where α is the mean depth of rainfall events. Since the model is interpreted at the daily time scale, α may be estimated as the mean daily rainfall in days when precipitation occurs. In the following we will often refer to the value of the mean rainfall depth normalized by the active soil depth, i.e.,

$$\frac{1}{\gamma} = \frac{\alpha}{nZ_r}. \tag{2.8}$$

Both the Poisson process and the exponential distribution are of common use in simplified models of rainfall at a daily time scale. The exponential distribution fits daily rainfall data well and, at the same time, allows analytical tractability (Benjamin and Cornell, 1970; Eagleson, 1978a, 1978b).

Notice that the rainfall rate $R(t)$ in Eq. (2.4) can be linked to the probability distributions Eqs. (2.6) and (2.7) if one expresses the marked Poisson process as a temporal sequence, i.e.,

$$R(t) = \sum_i h_i \delta(t - t_i) \tag{2.9}$$

where $\delta(\cdot)$ is the Dirac delta function, $\{h_i, i = 1, 2, 3, \ldots\}$ is the sequence of random rainfall depths with distribution given by Eq. (2.7), and $\{\tau_i = t_i - t_{i-1}, i = 1, 2, 3, \ldots\}$ is the interarrival time sequence of a stationary Poisson process with rate λ.

For the moment, the values of α and λ are assumed to be time-invariant quantities, representative of a typical growing season. In cases where there are significant changes in the parameters throughout the season, it may be useful to consider the early growing and the late growing seasons separately, each one with its own set of parameters. Chapter 8 will deal with seasonal and inter-annual variability of α and λ.

2.1.2 Interception

Part of the rainfall is intercepted by the aerial part of vegetation, while the remaining directly reaches the soil as throughfall (Figure 2.1). Especially in arid and semi-arid climates, where rainfall events are generally short and evaporation demand is high, a sizeable fraction of the intercepted rainfall is lost directly through evaporation, while the rest reaches the soil as stem flow (e.g., Dingman, 1994; Scholes and Archer, 1997; Waring and Running, 1998). The precise mechanisms of interception are quite complicated to model and depend on vegetation type as well as on the intensity and duration of rainfall. Because of its strong dependence on the type of plant and more specifically on its leaf area index, the amount lost by interception can indeed be quite different for, say, trees and grasses. As an example, well-vegetated trees in South African savannas can intercept up to over 0.2 cm of rainfall per storm event (Scholes and Walker, 1993), while grasses usually intercept much less. At small spatial scales interception is also known to alter the spatial distribution of the water reaching the soil (e.g., through stem flow and crown shading; Scholes and Archer, 1997), but these effects are not considered here.

In order to keep analytical tractability, interception is incorporated in the stochastic model by simply assuming that, depending on the kind of vegetation, a given amount of water can be potentially intercepted from each rainfall event (Rodríguez-Iturbe et al., 1999a). This implies fixing a threshold for rainfall depth, Δ, below which no water reaches the ground. If the depth of a given rainfall event, h_i, is higher than Δ, then the actual rainfall depth reaching the soil, h', is assumed to be $h_i - \Delta$, and Δ is lost by interception. The amount of water intercepted can be related to the type of vegetation by simply using different values for Δ. This model of interception is sketched in Figure 2.2a. The effect of fluctuations in wind and air temperature on

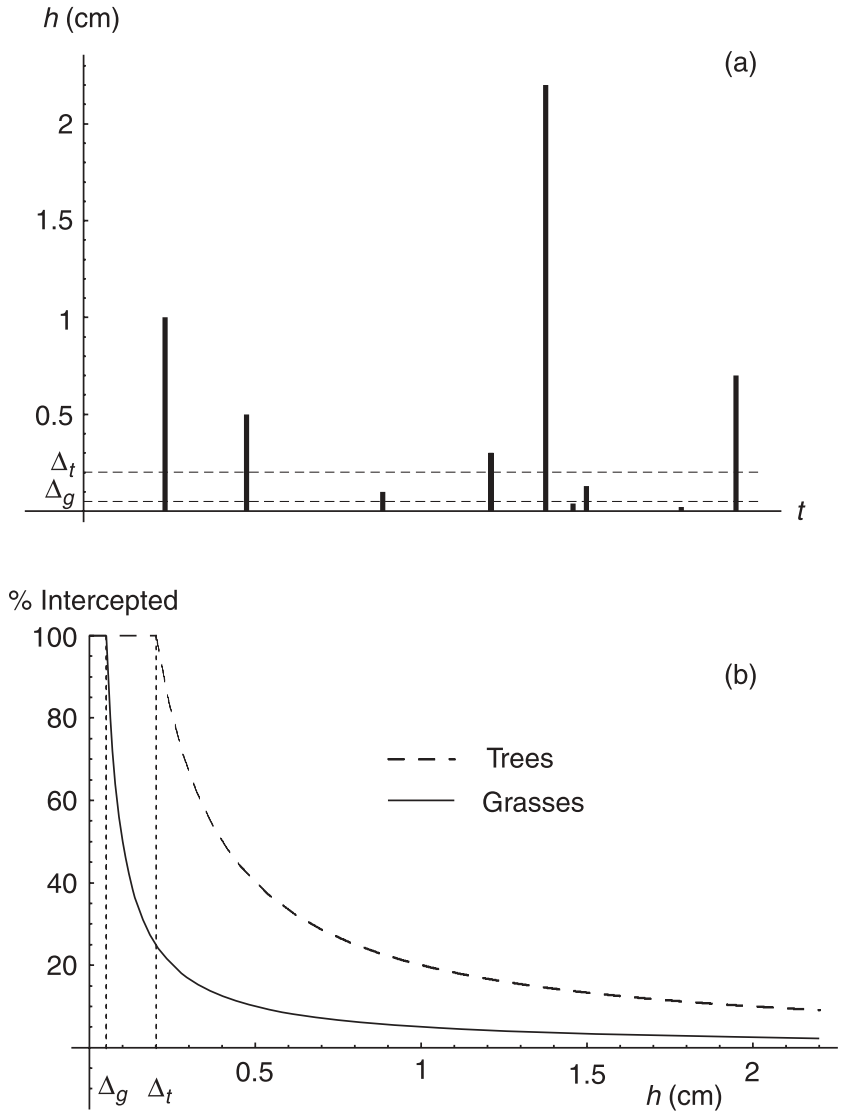

Figure 2.2 Representation of the modeling scheme adopted for interception. (a) Temporal sequence of rainfall events (h is the rainfall depth) along with the thresholds of interception, $\Delta_t = 0.2\,\text{cm}$ and $\Delta_g = 0.05\,\text{cm}$, typical for trees and grasses in some savannas. (b) Percentage of intercepted rainfall as a function of the total rainfall per event. After Laio et al. (2001a).

interception losses is assumed to be negligible compared to the role of differences in canopy coverage.

Although admittedly being a simplistic model for interception, the previous scheme provides a representation of the process that is in good agreement with the experimental evidence. As shown in Figure 2.2b, the percentage of rainfall intercepted as a function of total rainfall reproduces quite well the one found in field experiments (e.g., Feddes, 1971; Lai and Katul, 2000).

From a mathematical viewpoint the consideration of a threshold on the rainfall Poisson process does not complicate its analytical tractability. The

rainfall process is in fact transformed into a new marked-Poisson process, called a censored process, where the frequency of rainfall events is now

$$\lambda' = \lambda \int_{\Delta}^{\infty} f_H(h)\, \mathrm{d}h = \lambda \mathrm{e}^{-\Delta/\alpha} \tag{2.10}$$

and the depths h' have the same distribution as h, given by Eq. (2.7).Thus, one can simply write

$$R(t) - I(t) = \sum_i h'_i \delta(t - t'_i) \tag{2.11}$$

where $\{\tau'_i = t'_i - t'_{i-1}, i = 1, 2, 3, \ldots\}$ is the interarrival time sequence of a stationary Poisson process with frequency λ'.

2.1.3 Infiltration and runoff

When the soil has enough available storage to accommodate all the incoming water of the rainfall event, the increment in water storage is equal to the rainfall depth of the event; whenever the rainfall depth exceeds the available storage, the excess is converted into surface runoff. Since it depends on both rainfall and soil moisture content, infiltration from rainfall is a stochastic, state-dependent component, whose magnitude and temporal occurrence are controlled by the entire soil moisture dynamics. Because of the vertically lumped representation of soil moisture dynamics, the temporal propagation of the wetting front into the soil is not considered. However, this is not judged to be too restrictive when the soil moisture dynamics is considered at the daily time scale. Chapter 9 addresses the conditions of validity and the degree of approximation of such a hypothesis.

The probability distribution of the infiltration component may be easily written in terms of the exponential rainfall-depth distribution of Eq. (2.7) and the soil moisture state s. Referring to its dimensionless counterpart y (i.e., the infiltrated depth of water normalized by nZ_{r}) one can write

$$f_Y(y, s) = \gamma \mathrm{e}^{-\gamma y} + \delta(y - 1 + s) \int_{1-s}^{\infty} \gamma \mathrm{e}^{-\gamma u}\, \mathrm{d}u, \quad \text{for} \quad 0 \le y \le 1 - s, \tag{2.12}$$

where γ is defined in Eq. (2.8). Equation (2.12) is thus the probability distribution of having a jump in soil moisture equal to y, starting from a level s. The mass at $(1 - s)$ represents the probability that a storm will produce saturation when the soil has moisture s (Figure 2.3). This sets the upper

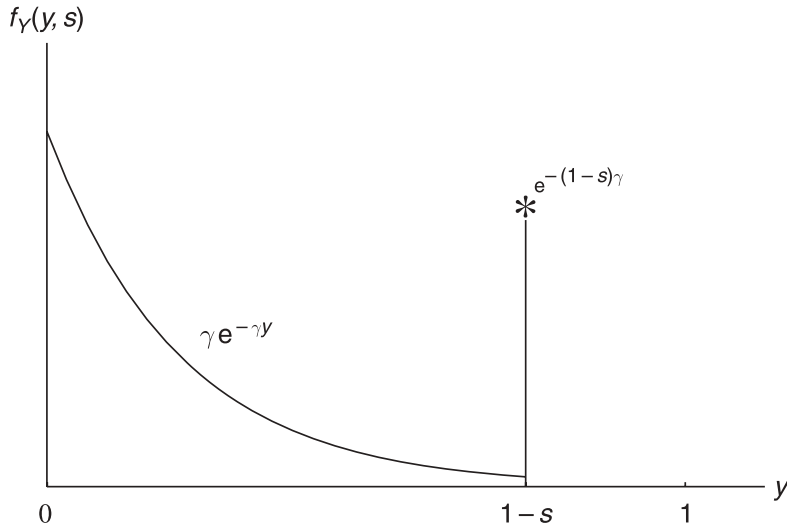

Figure 2.3 Sketch of the probability density function describing infiltration from rainfall y. The asterisk represents the atom of probability corresponding to soil saturation. After Rodriguez-Iturbe et al. (1999a).

bound of the process at $s = 1$, making the soil moisture balance evolution, e.g., Eq. (2.3), a bounded shot noise process. Although the bounded character of the process complicates its mathematical analysis, it will be seen that the Markovian nature of the process allows for a complete analytical solution in the case of steady-state conditions.

Similarly to Eq. (2.11), infiltration from rainfall can be written in Eq. (2.3) as

$$\varphi[s(t), t] = nZ_r \sum_i y_i \delta(t - t_i') \tag{2.13}$$

where $\{y_i, i = 1, 2, 3, \ldots\}$ is the sequence of random infiltration events having a distribution as in Eq. (2.12).

The probabilistic analysis of the temporal distribution of runoff production requires the study of the crossing properties of the level $s = 1$, using the framework discussed in the next chapter. It is only noted here that the runoff process by itself is not Markovian and that the temporal distribution of its time of occurrence is not exponential. It is also worth noting that runoff production may be interpreted in a different but equivalent manner by considering an alternative process where runoff occurs from deterministic losses that take place at an infinite rate above $s = 1$. In this case the state variable s is not required to be formally bounded at $s = 1$, as the instantaneous decay above $s = 1$ makes the process completely equivalent to the bounded one for $s < 1$. This interpretation will turn out to be useful for a more intuitive interpretation of some of the results that will be presented later.

2.1.4 Active soil depth

The soil is modeled as a horizontal layer of depth Z_r with homogeneous characteristics. As previously defined, the product of soil depth and porosity gives the active soil depth, nZ_r, which is the height (or volume per unit surface area) available for water storage. From a physical viewpoint, the active soil depth in Eq. (2.3) controls the response time of the system. As will be seen in detail later, different values of nZ_r greatly affect the interaction of soil and vegetation with the climate forcing. It is interesting to point out how the intermittent nature of the forcing, which makes the system undergo continuous fluctuations, leads to the aforementioned role of the active soil depth, even in statistically steady conditions. From a mathematical viewpoint, this important interplay between temporal forcing and soil depth can be understood from Eq. (2.3), in that if the infiltration from rainfall were constant in time instead of intermittent, the steady-state condition would be independent of soil depth.

The values of porosity and soil depth are generally influenced by many factors. Porosity usually shows some dependence on soil texture; plant roots and the action of small animals may also alter the value of the so-called macroporosity and produce preferential directions for water movement. However, since the effective importance of these latter variations of porosity is difficult to quantify without making the modeling scheme restrictively specific, we will refer only to variations due to different soil textures (see Table 2.1). The actual soil depth involved in the water balance is a difficult parameter to estimate and may show a large range of spatial variation, depending on soil pedology and, especially, vertical root distribution (e.g., Canadell et al., 1996; Jackson et al., 1996; Schulze et al., 1996). As a general rule, trees generally have deeper roots than grasses, and tend to be accompanied by a slightly higher effective porosity.

A number of links and feedbacks between vegetation, climate, and soil will not be considered, being of secondary importance at the time scale of concern. However, for analyses focusing on the long-term dynamics of vegetation, the variations of porosity, soil aging, and soil depth, which are linked to soil production and in turn also to soil moisture dynamics, should be taken into account. Such variations generally take place at much longer time scales than the ones considered here, but can become faster in tropical ecosystems (Larcher, 1995; see also Chapter 10). In those cases, nZ_r and the other soil characteristics may not be considered static parameters, but evolving variables.

The relevance of the active soil depth in regard to its role in large-scale soil moisture dynamics and its relevant ecological consequences will be evident

Table 2.1 *Parameters describing the soil characteristics used in the model for five different soil textures. After Laio et al. (2001a).*

	$\overline{\Psi}_s$ (MPa)	b	c	K_s (cm day^{-1})	n	β	s_h	s_w	s^*	s_{fc}
Sand	$-0.34 \cdot 10^{-3}$	4.05	11.1	> 200	0.35	12.1	0.08	0.11	0.33	0.35
Loamy sand	$-0.17 \cdot 10^{-3}$	4.38	11.7	≈ 100	0.42	12.7	0.08	0.11	0.31	0.52
Sandy loam	$-0.70 \cdot 10^{-3}$	4.90	12.8	≈ 80	0.43	13.8	0.14	0.18	0.46	0.56
Loam	$-1.43 \cdot 10^{-3}$	5.39	13.8	≈ 20	0.45	14.8	0.19	0.24	0.57	0.65
Clay	$-1.82 \cdot 10^{-3}$	11.4	25.8		0.5	26.8	0.47	0.52	0.78	≈ 1

Data from Harr (1962); De Wiest (1969); Clapp and Hornberger (1978); Cosby et al. (1984); Dingman (1994).
$\overline{\Psi}_s$ is the geometric mean of different measurements (Clapp and Hornberger, 1978).
s_h, s_w, and s^* correspond to Ψ_s of -10, -3, -0.03 MPa, respectively.

throughout the entire book. Milly and Dunne (1993) and Milly (1997) have also studied the effect of soil depth on the global water balance and its response to climate change. Nepstad et al. (1994), Canadell et al. (1996), and Scholes and Archer (1997) have dealt with the impact of soil depth on plant water stress and on the possible selection of temporal niches of soil moisture availability by different vegetation types.

2.1.5 Evapotranspiration

Since interception has already been subtracted (e.g., Eq. (2.11)), the term $E[s,(t)]$ in Eq. (2.5) represents the sum of the losses resulting from plant transpiration and evaporation from the soil. Although these are governed by different mechanisms, we will consider them together for the moment.

When soil moisture is high, the evapotranspiration rate depends mainly on the type of plant and climatic conditions (e.g., leaf area index, wind speed, air temperature and humidity, etc.). As long as soil moisture content is sufficient to permit the normal course of the plant physiological processes, evapotranspiration is assumed to occur at a maximum rate E_{max}, which is independent of s. When soil moisture content falls below a given point s^*, which depends on both vegetation and soil characteristics, plant transpiration (at the daily time scale) is reduced by stomatal closure to prevent internal water losses and soil water availability becomes a key factor in determining the actual evapotranspiration rate (e.g., Schulze, 1986; Hale and Orcutt, 1987; Smith and Griffith, 1993; Larcher, 1995; Nilsen and Orcutt, 1998; see also Chapters 4 and 6). Transpiration and root water uptake continue at a reduced rate until soil moisture reaches the so-called wilting point s_w.[1] At this level, suction to extract water from soil is so high that it damages the plant tissues (e.g., Lange et al., 1976; Schulze, 1986; Nilsen and Orcutt, 1998). Small water losses from the plant continue via cuticular transpiration and, if soil water is not replenished by rainfall, wilting and irreversible plant damage begin to appear (plant water stress is discussed in detail in Chapter 4). Below wilting point, s_w, soil water is further depleted only by evaporation at a very low rate up to the so-called hygroscopic point, s_h.

It will be seen in Chapters 4 and 6 that below s^* the rate of transpiration is reduced by a series of complex mechanisms and feedbacks, exerted at different

[1] We note that s^* and s_w are two very important thresholds used to describe in a practical manner the behavior of transpiration as a function of soil moisture at the daily time scale. Apart from that, however, they do not have a specific physical meaning and the fact that they are often referred to as the "point of incipient stomatal closure" and "the wilting point" respectively should not be misleading in this respect. The climate, soil, and vegetation characteristics controlling their values will be discussed in Chapter 6.

levels in the soil–plant–atmosphere continuum. The resulting relationship between the transpiration and soil moisture content in the range between s^* and s_w is well approximated by a linear decrease (e.g., Schulze, 1986; Hale and Orcutt, 1987). Figure 2.4 shows an example of the relationship between leaf (or stomatal) conductance and soil moisture content measured during a controlled experiment. The strongly nonlinear, threshold-like dependence on soil

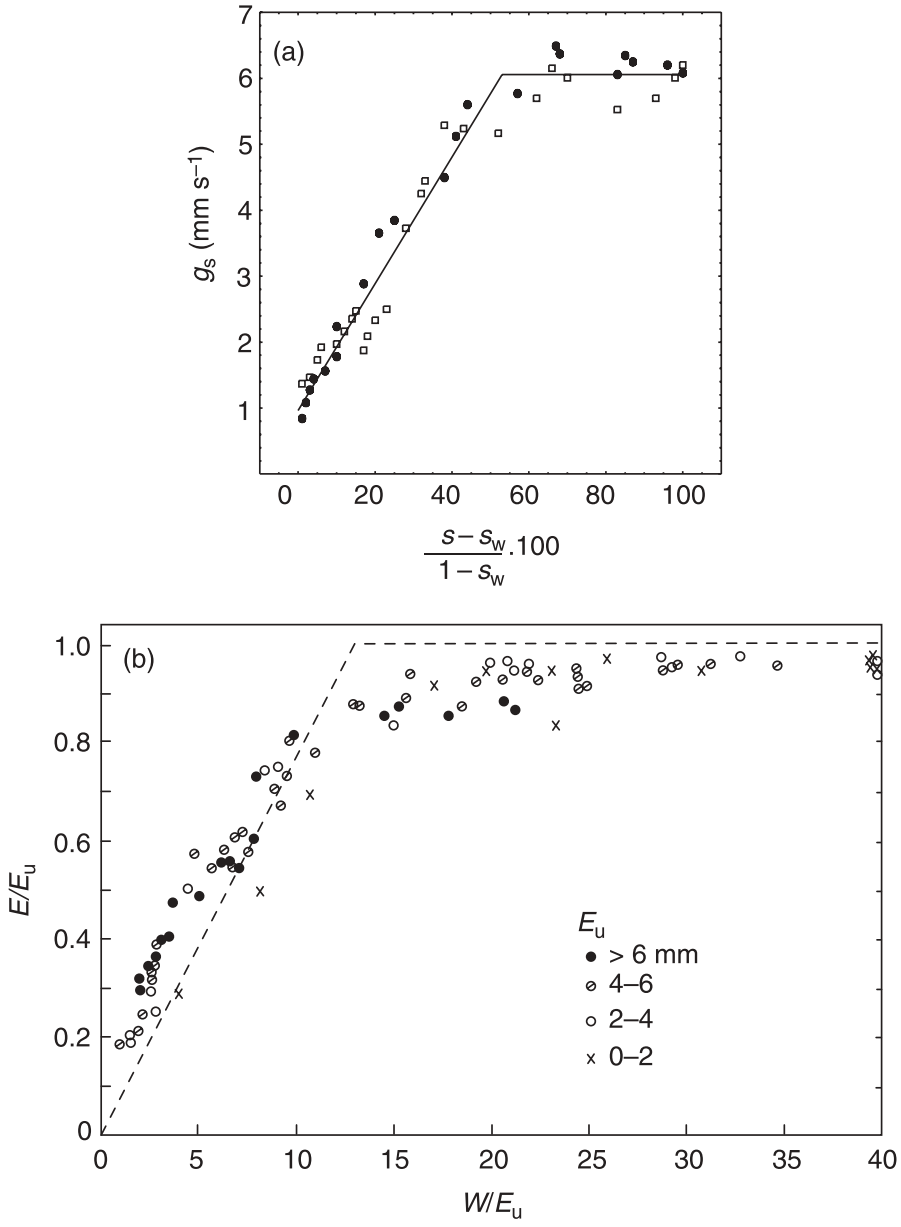

Figure 2.4 (a) Leaf stomatal conductance, g_s, versus soil moisture level for *Nerium oleander*, measured maintaining two different levels of vapor pressure deficit (solid circles and open squares, respectively). Adapted from Schulze (1986) and after Gollan et al. (1985). (b) Normalized daily transpiration as a function of available soil moisture from simulation and data of stressed yellow birch. E is the daily transpiration (mm), E_u is the unstressed daily transpiration (mm), and W is the available water in the root zone (mm). After Federer (1979); see also Federer and Gee (1976).

moisture is clearly evident. Notice also from Figure 2.4 that the soil moisture level at which stomatal closure begins is not very sensitive to changes in vapor pressure deficit. Since leaf conductance exerts the most important control on transpiration (transpiration rate is practically proportional to leaf conductance; see Chapter 6), the same kind of dependence on soil moisture is also true for transpiration (e.g., Jones, 1992; Nobel, 1999), as clearly shown in the example of Figure 2.4b. For most plants in temperate and semi-arid regions, this typical behavior at the daily time scale, can be found in the literature at the level both of the single plant and of the entire stand (e.g., Gardner and Ehlig, 1963; Federer, 1979; Spittlehouse and Black, 1981; Federer, 1982; Schulze, 1993; Paruelo and Sala, 1995; Williams and Albertson, 2004). The origin of this dependence on soil moisture will be investigated in detail in Chapter 6, where the hourly transpiration course will be integrated to the daily time scale. Due to different and specialized photosynthetic pathways (e.g., the CAM pathway), notable exceptions to this behavior in extremely arid regions have been reported (e.g., MacMahon and Schimpf, 1981; Larcher, 1995), so that suitable modifications should be considered for the analogous modeling of transpiration-vs-soil moisture in particular species of desert flora.

From the above arguments, daily evapotranspiration losses will be assumed to happen at a constant rate E_{max} for $s^* < s < 1$, and then to linearly decrease with s, from E_{max} to a value E_w at s_w. Below s_w, only evaporation from the soil is present and the loss rate is assumed to decrease linearly from E_w to zero at s_h. The dependence of evapotranspiration losses on soil moisture is thus summarized in the following expression

$$E(s) = \begin{cases} 0 & 0 < s \leq s_h \\ E_w \frac{s - s_h}{s_w - s_h} & s_h < s \leq s_w \\ E_w + (E_{max} - E_w) \frac{s - s_w}{s^* - s_w} & s_w < s \leq s^* \\ E_{max} & s^* < s \leq 1, \end{cases} \tag{2.14}$$

whose behavior is shown in Figure 2.5.

As the smallest time scale of interest here is the daily scale, E_{max} can be interpreted as the average daily evapotranspiration of a unitary surface uniformly covered with vegetation under well-watered conditions during the growing season. Possible estimates of E_{max} values may be obtained using physically based expressions, such as the Penman–Monteith equation (see Chapter 6). However, in the following we prefer to refer to measured data, as is done, for example, by Paruelo and Sala (1995). For regions with hot growing seasons, values of E_{max} are typically around 0.5 cm day^{-1} for grasses

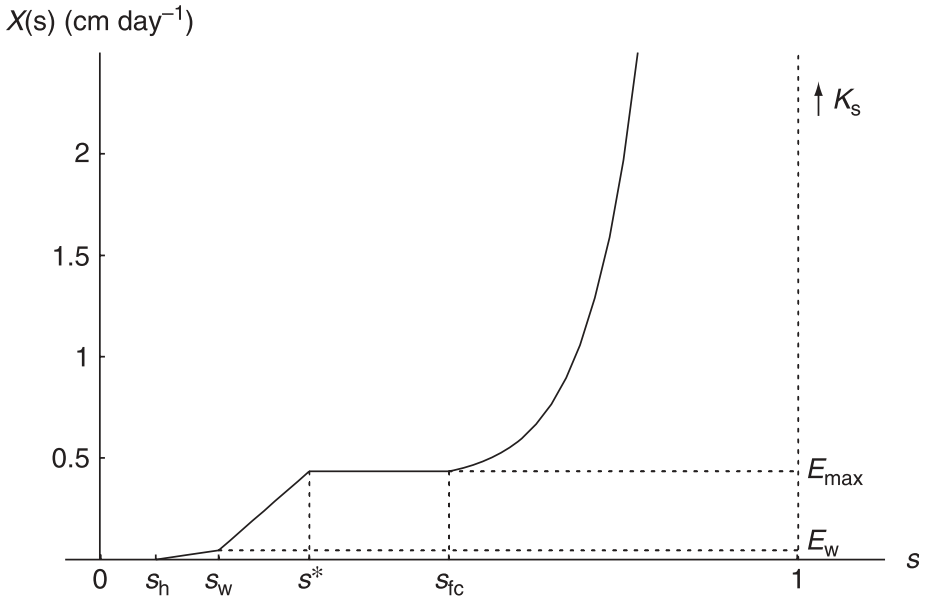

Figure 2.5 Soil water losses (evapotranspiration and leakage), $\chi(s)$, as a function of relative soil moisture for typical climate, soil, and vegetation characteristics in semi-arid ecosystems. After Laio et al. (2001a).

and 10% less for trees under well-watered conditions, although there is considerable variability among different plants and regions (e.g., data from Scholes and Walker, 1993). Of this total value approximately 0.1 cm day^{-1} can be attributed to evaporation from the soil (e.g., Nobel, 1999, page 360). The higher maximum transpiration rate of grasses in these regions is partly explained by the more efficient C_4 pathway of photosynthesis that many grasses of semi-arid ecosystems have with respect to the more common and less efficient C_3 pathway of trees.[2]

Chapter 6 will clarify how both the value of soil moisture, s^*, at which transpiration starts being reduced and the wilting point, s_w, depend on the type of vegetation and soil properties. An indication of their possible values can be obtained from the soil–plant–atmosphere continuum scheme, which describes the transfer of water by plants from soil to the atmosphere in terms of the water potential, Ψ, defined as the difference in free energy per unit volume evaluated with respect to that of pure water at zero reference level and under standard temperature and pressure conditions (e.g., Slatyer, 1967; Oertli, 1976; Larcher,

[2] In the so-called C_3 plants the primary product of the photosynthesis is a three-carbon sugar, while in C_4 species it is a four-carbon compound (see Chapter 6). As opposed to C_3 plants, in C_4 plants carbon dioxide and oxygen do not compete for the same enzyme, so that the higher rate of CO_2 fixing leads to concentrations of carbon dioxide inside the stomata that are much lower than those of C_3 species. This is generally associated with higher photosynthetic rates and water-use efficiencies for C_4 plants (Campbell and Norman, 1998). The biochemical and physiological differences between C_3 and C_4 plants have important consequences for ecological and hydrological processes. Regions with warm season rainfall tend to have greater C_4 abundance than do regions with cool season precipitation (Larcher, 1995; Lambers et al., 1998).

1995; Nobel, 1999). Assuming that any given plant is characterized by typical levels of plant water potential below which evapotranspiration is reduced and finally stopped, and considering that the daily averaged plant water potential is related to soil matrix potential (see Chapters 4 and 6), for each type of plant the typical values of soil matrix potential, Ψ_{s,s^*} and Ψ_{s,s_w}, at which stomatal closure begins and is completed, can be determined.

In general, wilting points for plants in water-controlled ecosystems are considerably lower than the value of −1.5 MPa commonly assumed for temperate crops. For plants in semi-arid environments, typical values of soil matrix potential at the wilting point, Ψ_{s,s_w}, can be as low as −3 MPa or even −5 MPa (e.g., Ludlow, 1976; Richter, 1976; MacMahon and Schimpf, 1981; Scholes and Walker, 1993; Larcher, 1995). There is considerable variation among different plants, but the permanent wilting point is frequently lower for grasses than for trees, even though grasses reach water stress conditions before trees do. There are fewer available data for Ψ_{s,s^*}, which in some water-restricted ecosystems is estimated to be around −0.03 MPa, with values somewhat larger for grasses than for trees (e.g., Scholes and Walker, 1993).

Soil matrix potential can be related to relative soil moisture using the soil-water retention curves (e.g., Clapp and Hornberger, 1978; Dingman, 1994; Hillel, 1998). Such curves depend on the type of soil and provide the dependence of s^* and s_w on soil texture. Following Clapp and Hornberger (1978) one can use empirically determined soil-water retention curves of the form

$$\Psi_s = \overline{\Psi}_s s^{-b} \tag{2.15}$$

where $\overline{\Psi}_s$ and b are experimentally determined parameters (see Table 2.1). Typical curves for loamy sand and loam are shown in Figure 2.6. It is worth noting that in order to obtain values of s_w and s^* in reasonable agreement with measured field data, one should use $\overline{\Psi}_s$ as given by the geometric mean of the measured values (reported by Clapp and Hornberger, 1978, page 603) instead of its arithmetic mean, which would yield unrealistically high values of soil moisture. As can be seen from Figure 2.6, the role of soil texture is very important. Different types of soil may yield very different levels of relative soil moisture corresponding to the same value of soil matrix potential. Typical values of s_w are found around 0.1 for loamy sand, while for loam they are near 0.25. Similarly, s^* is found to be around 0.3 for loamy sand and moves to above 0.55 in the case of loam (see Table 2.1). The values of s_w and s^* are crucially important both in the water balance and in the study of plant water stress. The above discussion clearly shows how the control of transpiration by vegetation,

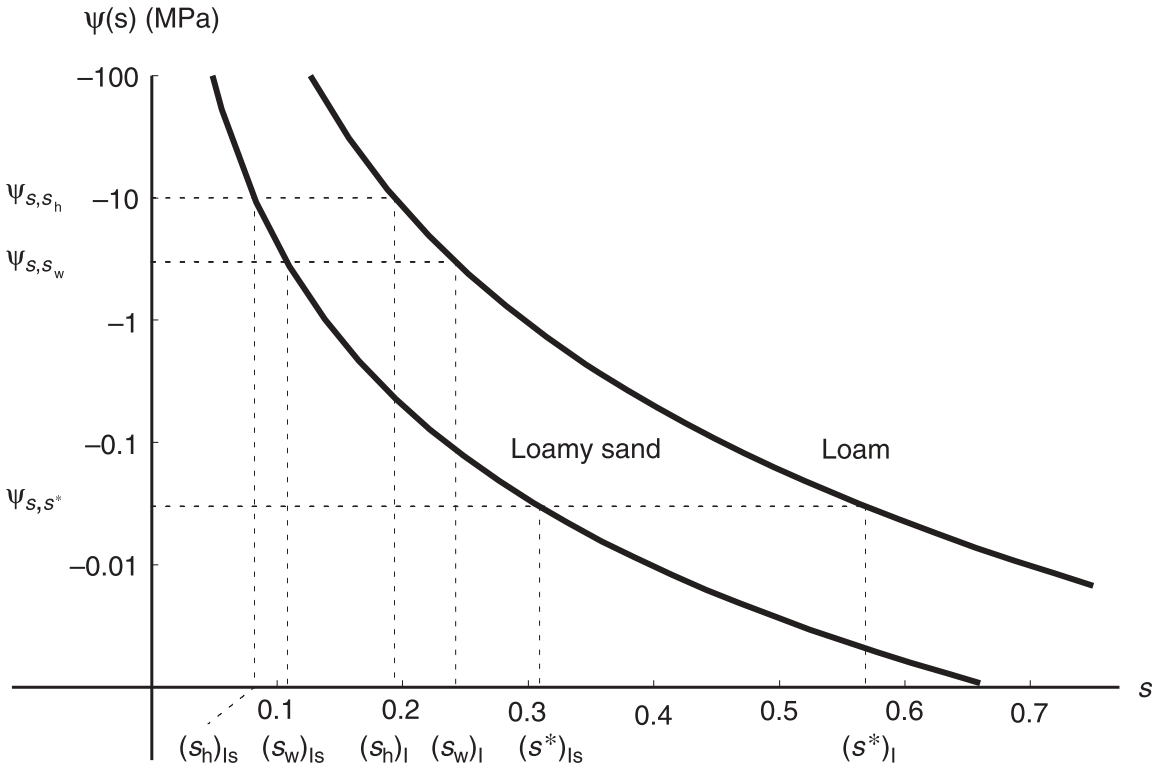

Figure 2.6 Soil moisture retention curves used to derive values of the soil water levels s_h, s_w, and s^* from the corresponding values of soil matrix potential, $\Psi_{s,s_h} = -10$ MPa, $\Psi_{s,s_w} = -3$ MPa, $\Psi_{s,s^*} = -0.03$ MPa. Two different soil types, a loamy sand (ls) and a loam (l), are considered, using the parameters reported in Table 2.1. After Laio et al. (2001a).

besides depending on physiological plant characteristics, relies directly on soil properties.

Thanks to the relatively small losses involved at low soil moisture levels, a precise evaluation of the values of E_w and s_h is not very important for the temporal evolution of the soil moisture process and the different components of water balance, as long as an approximately correct order of magnitude is used in their description. A reference value of -10 MPa will be used for Ψ_{s,s_h} and 0.01 cm day^{-1} for E_w. The value of s_h can be obtained from Ψ_{s,s_h} using the soil-water retention curves in the same way as for s_w and s^* (see Figure 2.6).

A final comment is in order concerning the temporal interplay of rainfall and evapotranspiration. The fact that evapotranspiration is considerably reduced during precipitation events would be a source of further complication if one considered the specific temporal dynamics within the rainfall event. This, however, is not relevant in the present model since rainfall is modeled as a sequence of instantaneous pulses, while evapotranspiration takes place continuously. Thus in our mathematical framework the instantaneous contribution of evapotranspiration is infinitesimal compared to that of rainfall in

Eq. (2.3) whenever there is a precipitation event. This might lead to a slight overestimation of the total evapotranspiration.

2.1.6 Leakage losses

Leakage losses are assumed to happen by gravity at the lowest boundary of the soil layer, neglecting possible differences in matrix potential between the soil layer under consideration and the one immediately below. The loss rate is assumed to be at its maximum when soil is saturated and then rapidly decays as the soil dries out, following the decrease of the hydraulic conductivity $K(s)$. The decay of the hydraulic conductivity is usually modeled using empirical relationships of different forms (e.g., Sisson et al., 1988; Hillel, 1998). Here the hydraulic conductivity is assumed to decay exponentially from a value equal to the saturated hydraulic conductivity K_s at $s = 1$, to a value of zero at a field capacity, s_{fc}. The exponential form, chosen for reasons of mathematical tractability, has been commonly employed in the literature (e.g., Davidson et al., 1963; Cowan, 1965; Sisson et al., 1988) as an alternative to the more customary power law. The assumed behavior of leakage losses is thus expressed as

$$L(s) = K(s) = \frac{K_s}{e^{\beta(1-s_{fc})} - 1}\left[e^{\beta(s-s_{fc})} - 1\right], \quad s_{fc} < s \leq 1, \tag{2.16}$$

where β is a coefficient that is used to fit the above expression to the power law (e.g., Clapp and Hornberger, 1978; Dingman, 1994; Hillel, 1998)

$$K(s) = K_s s^c, \tag{2.17}$$

with $c = 2b + 3$ and b defined in Eq. (2.15). A possible criterion to minimize the discrepancies between the two expressions (2.16) and (2.17) is to impose the condition that they subtend the same area between s_{fc} and $s = 1$. This provides $\beta = 2b + 4$ so that the value of β depends on the type of soil, varying from $\simeq 12$ for sand to $\simeq 26$ for clay. Using the typical values reported in Table 2.1, the two expressions have very similar behavior. The behavior of leakage losses is represented in Figure 2.5. The strong nonlinear behavior of these losses as a function of soil moisture content is evident in $\chi(s)$ for $s_{fc} \leq s \leq 1$.

The field capacity s_{fc} is the soil moisture content at which drainage by gravity practically ceases to occur (for a discussion of its physical and practical relevance see Hillel, 1998; see also footnote 1 of Section 2.1.5). Here it is operationally defined as the value of soil moisture at which the hydraulic conductivity according to Eq. (2.17) becomes negligible (10%) compared to

the maximum daily evapotranspiration losses, $E_{\max}$ (for this purpose fixed at $0.5\,\mathrm{cm\ day^{-1}}$).

From a physical viewpoint, the modeling of leakage driven by a unit vertical gradient due to gravity implies no interaction with the underlying soil layers and the water table. Such simplification may pose some restrictions in the use of the model, even though in most water-controlled ecosystems the contribution due to capillary rise from the water table or deeper soil layers, if any, is generally of secondary importance.

2.1.7 Soil-drying process

During interstorm periods the model Eq. (2.3) describes deterministic decays of soil moisture starting from initial values that depend on the previous history of the entire process. Upon normalization with respect to the active soil depth, the complete form of the losses described before is

$$\rho(s) = \frac{\chi(s)}{nZ_{\mathrm{r}}} = \frac{E(s) + L(s)}{nZ_{\mathrm{r}}} = \begin{cases} 0 & 0 < s \le s_{\mathrm{h}} \\ \eta_{\mathrm{w}} \frac{s - s_{\mathrm{h}}}{s_{\mathrm{w}} - s_{\mathrm{h}}} & s_{\mathrm{h}} < s \le s_{\mathrm{w}} \\ \eta_{\mathrm{w}} + (\eta - \eta_{\mathrm{w}}) \frac{s - s_{\mathrm{w}}}{s^* - s_{\mathrm{w}}} & s_{\mathrm{w}} < s \le s^* \\ \eta & s^* < s \le s_{\mathrm{fc}} \\ \eta + m\left[\mathrm{e}^{\beta(s - s_{\mathrm{fc}})} - 1\right] & s_{\mathrm{fc}} < s \le 1, \end{cases} \tag{2.18}$$

where $\rho(s)$ stands for the normalized loss function to which we will refer hereafter, and

$$\eta_{\mathrm{w}} = \frac{E_{\mathrm{w}}}{nZ_{\mathrm{r}}}, \tag{2.19}$$

$$\eta = \frac{E_{\max}}{nZ_{\mathrm{r}}}, \tag{2.20}$$

$$m = \frac{K_{\mathrm{s}}}{nZ_{\mathrm{r}}\left[\mathrm{e}^{\beta(1 - s_{\mathrm{fc}})} - 1\right]}. \tag{2.21}$$

Before studying the probabilistic structure of the overall process, it is useful to analyze the behavior of the system when undergoing a prolonged drought

following a rainy period. The analytical expression for the soil moisture decay from an initial condition $s_0 \geq s_{\mathrm{fc}}$ in the absence of rainfall events is

$$s(t) = \begin{cases} s_0 - \frac{1}{\beta} \ln \left\{ \frac{\left[\eta - m + m e^{\beta(s_0 - s_{\mathrm{fc}})}\right] e^{\beta(\eta - m)t} - m e^{\beta(s_0 - s_{\mathrm{fc}})}}{\eta - m} \right\} & 0 \leq t < t_{s_{\mathrm{fc}}} \\ s_{\mathrm{fc}} - \eta(t - t_{s_{\mathrm{fc}}}) & t_{s_{\mathrm{fc}}} \leq t < t_{s^*} \\ s_{\mathrm{w}} + (s^* - s_{\mathrm{w}}) \left[\frac{\eta}{\eta - \eta_{\mathrm{w}}} e^{-\frac{\eta - \eta_{\mathrm{w}}}{s^* - s_{\mathrm{w}}}(t - t_{s^*})} - \frac{\eta_{\mathrm{w}}}{\eta - \eta_{\mathrm{w}}} \right] & t_{s^*} \leq t < t_{s_{\mathrm{w}}} \\ s_{\mathrm{h}} + (s_{\mathrm{w}} - s_{\mathrm{h}}) e^{-\frac{\eta_{\mathrm{w}}}{s_{\mathrm{w}} - s_{\mathrm{h}}}(t - t_{s_{\mathrm{w}}})} & t_{s_{\mathrm{w}}} \leq t < \infty, \end{cases} \tag{2.22}$$

where

$$\begin{aligned} t_{s_{\mathrm{fc}}} &= \frac{1}{\beta(m - \eta)} \left\{ \beta(s_{\mathrm{fc}} - s_0) + \ln \left[\frac{\eta - m + m e^{\beta(s_0 - s_{\mathrm{fc}})}}{\eta} \right] \right\}, \\ t_{s^*} &= \frac{s_{\mathrm{fc}} - s^*}{\eta} + t_{s_{\mathrm{fc}}}, \\ t_{s_{\mathrm{w}}} &= \frac{s^* - s_{\mathrm{w}}}{\eta - \eta_{\mathrm{w}}} \ln \left(\frac{\eta}{\eta_{\mathrm{w}}} \right) + t_{s^*} \end{aligned} \tag{2.23}$$

represent the time to evolve, in the absence of rainfall, from s_0 to s_{fc}, s^*, and s_{w} respectively. Note that, since the moisture decays exponentially to s_{h}, the process will only be at $s = s_{\mathrm{h}}$ if it starts at that value.

Figures 2.7a and 2.7b show examples of Eq. (2.22) starting from saturated conditions. One can clearly see the remarkable control exerted by both the soil texture and the active soil depth. Under the same climatic conditions and with the same vegetation type (i.e., same $E_{\max}$, $\Psi_{\mathrm{s},s_{\mathrm{w}}}$, and Ψ_{s,s^*}) the time to reach the wilting point in the absence of precipitation can vary from around 20 days for a shallow loamy sand, up to well beyond 60 days for a deep loamy soil. It is also interesting to note the different effects of soil texture on the water availability for vegetation. On one hand, because of its lower hydraulic conductivity, a finer soil increases soil water availability and thus the time to reach the wilting point; on the other hand, the higher values of s_{h}, s_{w}, and s^* lead to an increase in the amount of residual water that is not extractable for plant transpiration.

2.2 Probabilistic evolution of the soil moisture process

The stochastic rainfall forcing in Eq. (2.3) makes its solution meaningful only in probabilistic terms. The probability density function of soil moisture, $p(s, t)$, can be derived from the Chapman–Kolmogorov forward equation for the process under analysis (Rodríguez-Iturbe et al., 1999a; see also Cox and Miller, 1965).

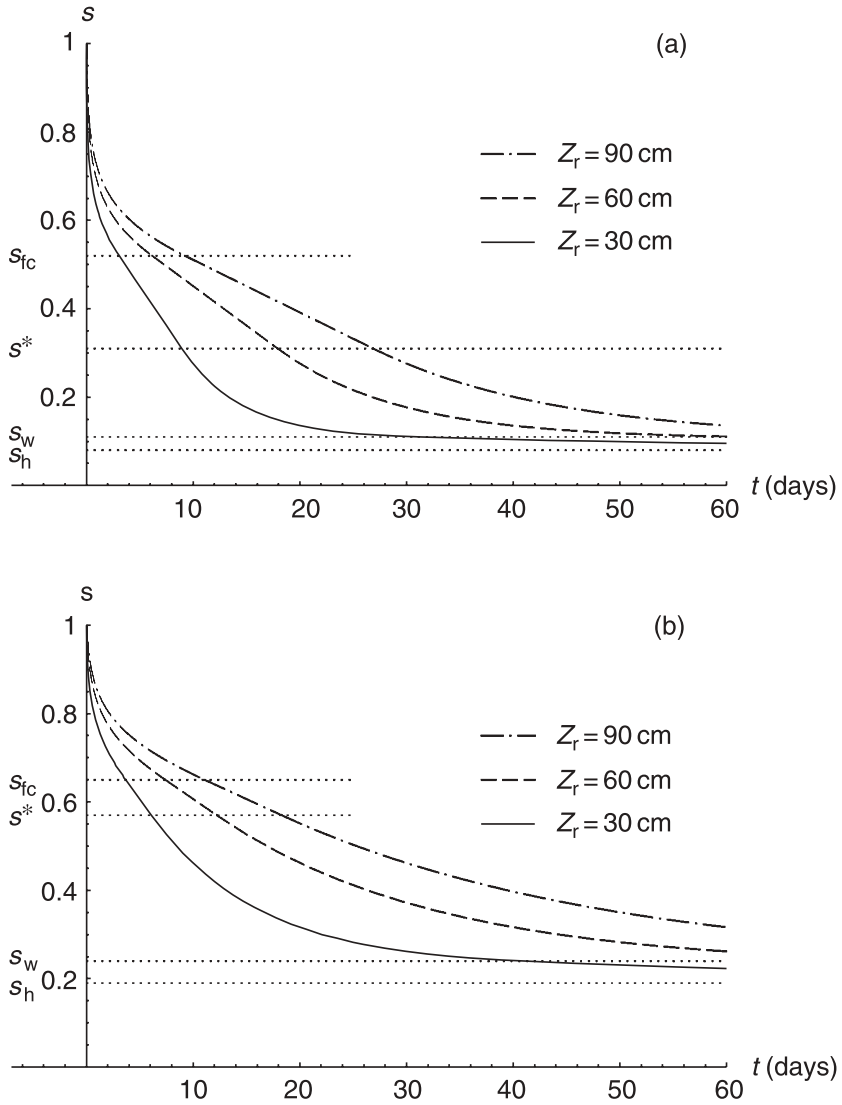

Figure 2.7 Plots of the solutions of the soil-drying process for a loamy sand (a) and loam (b) with different values of active soil depth (30, 60, and 90 cm). The parameters used are $E_{max} = 0.45$ cm day^{-1}, and $E_w = 0.01$ cm day^{-1}. The values of s_h, s_w, s^*, s_{fc}, n, β, and K_s are reported in Table 2.1. After Laio et al. (2001a).

Suppose that at time t the soil moisture level is $s(t)$ and consider a small time interval from t to $t + \Delta t$. The probability that no positive increment in soil moisture occurs is $1 - \lambda' \Delta t + o(\Delta t)$, where λ' is defined in Eq. (2.10). In this case soil moisture evolves deterministically as

$$s(t + \Delta t) = \begin{cases} s(t) - \Delta s & s(t) > \Delta s + s_h \\ s_h & s_h \leq s(t) \leq \Delta s + s_h, \end{cases} \tag{2.24}$$

where $\Delta s = \int_t^{t+\Delta t} \rho[s(\tau)] \mathrm{d}\tau = \rho[s(t)] \Delta t + o(\Delta t)$.

The probability that a positive increment in soil moisture takes place is $\lambda' \Delta t + o(\Delta t)$. In this case

$$s(t + \Delta t) = \begin{cases} s(t) + y - \Delta s & s(t) > \Delta s + s_h + y \\ s_h & s_h \leq s(t) \leq \Delta s + s_h + y, \end{cases} \tag{2.25}$$

where y is the normalized soil moisture increment governed by the probability distribution $f_Y(y, s)$ described by Eq. (2.12).

In general, at time t the distribution of $s(t)$ consists of a discrete atom of probability $p_0(t)$ that the soil is at $s = s_h$ and a density $p(s, t)$ for $s > s_h$. The probability that the soil moisture takes a value in $(s, s + \Delta s)$ at the time $t + \Delta t$ can therefore be expressed as follows (e.g., Cox and Miller, 1965, page 241)

$$\begin{aligned} p(s, t + \Delta t)\Delta s =& (1 - \lambda' \Delta t) p(s + \Delta s, t)\, \mathrm{d}(s + \Delta s) \\ &+ \lambda' \Delta t \int_{s_h}^{s} p(u + \Delta u, t)\, f_Y(s - u, u)\, \mathrm{d}(u + \Delta u)\, \mathrm{d}s \\ &+ \lambda' \Delta t p_0(t)\, f_Y(s - s_h, s_h)\Delta s + o(\Delta t). \end{aligned} \tag{2.26}$$

The first term on the r.h.s. of Eq. (2.26) describes the situation when the soil moisture reaches the value s at time $t + \Delta t$ given that no rainfall events have occurred in the interval Δt. The second term allows for the case when the soil moisture reaches s due to a positive increment resulting from the arrival of a rainfall event and the third term corresponds to the case when the process is at $s = s_h$ at time t and the arrival of a storm event makes the moisture content jump to s at time $t + \Delta t$.

Similarly, the atom of probability at s_h satisfies the equation

$$\begin{aligned} p_0(t + \Delta t) &= (1 - \lambda' \Delta t)\; p_0(t) + (1 - \lambda' \Delta t) \int_{s_h}^{\rho(s_h)\Delta t} p(u, t)\, \mathrm{d}u + o(\Delta t) \\ &= (1 - \lambda' \Delta t)\; [p_0(t) + p(s_h, t)\; \rho(s_h)\Delta t] + o(\Delta t), \end{aligned} \tag{2.27}$$

where the second term on the r.h.s. accounts for the probability of moving to $s = s_h$ from a value infinitesimally above it, in the absence of rain.

Substituting now for Δs and Δu in the r.h.s. of Eq. (2.26), one obtains

$$\begin{aligned} p(s, t + \Delta t)\Delta s =& (1 - \lambda' \Delta t)\; p[s + \rho(s)\Delta t, t]\, \mathrm{d}[s + \rho(s)\Delta t] \\ &+ \lambda' \Delta t \int_{s_h}^{s} p[u + \rho(u)\Delta t, t]\, f_Y(s - u, u)\, \mathrm{d}[u + \rho(u)\Delta t]\, \mathrm{d}s \\ &+ \lambda' \Delta t p_0(t)\, f_Y(s - s_h, s_h)\, \mathrm{d}s + o(\Delta t) \\ =& (1 - \lambda' \Delta t) \left[p(s, t) + \rho(s)\Delta t \frac{\partial}{\partial s} p(s, t) \right] \left[1 + \frac{\partial}{\partial s} \rho(s)\Delta t \right] \mathrm{d}s \\ &+ \lambda' \Delta t \Delta s \int_{s_h}^{s} p(u, t)\, f_Y(s - u, u)\, \mathrm{d}u \\ &+ \lambda' \Delta t \Delta s p_0(t)\, f_Y(s - s_h, s_h) + o(\Delta t). \end{aligned} \tag{2.28}$$

Finally, dividing by Δs, subtracting $p(s,t)$ from both sides, dividing by Δt, and taking the limit as $\Delta t \to 0$, one gets

$$\frac{\partial}{\partial t}p(s,t) = \frac{\partial}{\partial s}\left[p(s,t)\rho(s)\right] - \lambda' p(s,t) + \lambda' \int_{s_h}^{s} p(u,t)\, f_Y(s-u,u)\, \mathrm{d}u + \lambda' p_0(t)\, f_Y(s-s_h, s_h). \tag{2.29}$$

The various terms on the r.h.s. of the integro-differential Eq. (2.29) represent the contributions to $p(s,t)$ of the different mechanisms of the soil moisture process. The first term is related to the gain of probability due to the drift of the pdf in the deterministic decay caused by $\rho(s)$, the second term represents the loss of probability due to possible jumps with frequency λ' which cause the process to leave the given trajectory moving to the level s at time t, and the last term is the positive contribution to the probability due to jumps to level s starting from lower soil moisture values.

Similarly, taking the limit as $\Delta t \to 0$, Eq. (2.27) yields

$$\frac{\mathrm{d}}{\mathrm{d}t}p_0(t) = -\lambda' p_0(t) + \rho(s_h)p(s_h,t). \tag{2.30}$$

Equations (2.29) and (2.30) are the Chapman–Kolmogorov forward equations for the evolution of the probability of s and are similar to those of Cox and Isham (1986). They are valid for general choices of the loss function $\rho(s)$ and jump distribution $f_Y(y,s)$ and thus describe both the classic Takacs (1955) problem, where the jumps can be of any size, and the present case, where the state of the system is bounded, as follows from the particular distribution of jump given by Eq. (2.12). Notice that the bound at $s = 1$ does not produce a probability mass for the soil moisture process at $s = 1$, since the process decays immediately from that state. The reason for this lies in the fact that the input is in the form of an instantaneous pulse rather than a pulse with a finite duration (as in the case considered by Gani, 1955). A further consequence of the saturation at $s = 1$ is that the right hand tail of the pdf of the soil moisture does not necessarily decay to zero, but instead has $p(1,t) > 0$. Since the soil moisture losses approach zero at s_h in a continuous manner (see Eq. (2.18) and Figure 2.5), the soil moisture approaches s_h asymptotically and thus the process will only be at $s = s_h$ if it starts at that value (Figure 2.7). As a consequence, the probability distribution of the soil moisture has no atom p_0 except when the process starts at s_h.

2.3 Steady-state probability distribution of soil moisture

The complete solution of Eqs. (2.29) and (2.30) presents serious mathematical difficulties. Only formal solutions in terms of Laplace transforms have been

obtained for simple cases when the process is not bounded at $s = 1$ (Cox and Isham, 1986 and references therein). While some insights into the transient conditions for the soil moisture process will be given in Chapter 3 and in Sections 7.1 and 8.1, attention is focused here on the steady-state case.

Considering losses approaching zero at s_h in a continuous manner (Figure 2.5) the steady-state solution is continuous with no atom of probability at s_h. On taking the limit as $t \to \infty$ in Eqs. (2.29) and (2.30), one obtains

$$\frac{\mathrm{d}}{\mathrm{d}s}[\rho(s)p(s)] - \lambda' p(s) + \lambda' \int_{s_h}^{s} p(u)\, f_Y(s-u,u)\,\mathrm{d}u = 0, \tag{2.31}$$

which, using Eq. (2.12) yields

$$\begin{aligned}\frac{\mathrm{d}}{\mathrm{d}s}[\rho(s)p(s)] - \lambda' p(s) + \lambda' \int_{s_h}^{s} p(u)\gamma \mathrm{e}^{-\gamma(s-u)}\,\mathrm{d}u \\ + \delta(s-1)\lambda' \int_{s_h}^{s} p(u)\gamma \mathrm{e}^{-\gamma(1-u)}\,\mathrm{d}u = 0.\end{aligned} \tag{2.32}$$

For $s < 1$, the delta functions disappear in Eq. (2.32) and, after multiplying by $\mathrm{e}^{\gamma s}$ and differentiating with respect to s, it can be easily shown to be equivalent to the ordinary differential equation (Cox and Isham, 1986; Rodríguez-Iturbe et al., 1999a)

$$\frac{\mathrm{d}}{\mathrm{d}s}[\rho(s)p(s)] + \gamma\rho(s)p(s) - \lambda' p(s) = 0. \tag{2.33}$$

Comparing Eqs. (2.32) and (2.33) one also obtains

$$\rho(s)p(s) = \lambda' \int_{s_h}^{s} p(u)\, \mathrm{e}^{-\gamma(s-u)}\,\mathrm{d}u. \tag{2.34}$$

For $s = 1$, Eq. (2.32) becomes

$$\begin{aligned}p(1)\frac{\mathrm{d}}{\mathrm{d}s}\rho(s)\Big|_{s=1} - \rho(1)p(1)\delta(0) - \lambda' p(1) + \lambda' \int_{s_h}^{1} p(u)\gamma \mathrm{e}^{-\gamma(1-u)}\,\mathrm{d}u \\ + \delta(0)\lambda' \int_{s_h}^{1} p(u)\mathrm{e}^{-\gamma(1-u)}\,\mathrm{d}u = 0.\end{aligned} \tag{2.35}$$

Since $\rho(s)$ in 1 is continuous and therefore its derivative in 1 does not contain delta functions, by dividing Eq. (2.34) by $\delta(0)$ and neglecting the infinitesimal terms, one obtains

$$\gamma\rho(1)p(1) = \lambda' \int_{s_h}^{1} p(u)\, \mathrm{e}^{-\gamma(1-u)}\,\mathrm{d}u, \tag{2.36}$$

which turns out to be the same as Eq. (2.34) calculated in $s = 1$. Equations (2.33) and (2.34) are thus both valid for the bounded and unbounded case, whose solutions therefore only differ by an arbitrary constant of integration. Accordingly, the general form of the steady-state solution is easily obtained from Eq. (2.33) as

$$p(s) = \frac{C}{\rho(s)}\, \mathrm{e}^{-\gamma s + \lambda' \int \frac{\mathrm{d}u}{\rho(u)}} \qquad \text{for } s_{\mathrm{h}} < s \leq 1, \tag{2.37}$$

where C is the normalization constant such that

$$\int_{s_{\mathrm{h}}}^{1} p(s)\, \mathrm{d}s = 1. \tag{2.38}$$

Notice that all the complications brought by the presence of the bound at $s = 1$ are contained in the integration constant and the only effect of the saturation of the soil at $s = 1$ is the restricted range over which $p(s)$ is normalized in Eq. (2.38). The explanation for this lies in the Markovian nature of the soil moisture process (Rodríguez-Iturbe et al., 1999a). If excursions of the process above 1 are impossible, the process will spend more time in states $s \leq 1$ than would be the case otherwise, but the relative proportions of times in those states will be unchanged. Imagine two processes with, and without, the restriction that s is bounded to values less than 1. In the latter case, trajectories of the soil moisture process will jump above the level $s = 1$ and, eventually, drift down across this level once more. In the former case, these excursions are effectively excised, as the process jumps only to $s = 1$ and then immediately begins its downward decay. The trajectories below $s = 1$ in the two processes are indistinguishable.

The limits of the integral in the exponential term of Eq. (2.37) are chosen so as to assure the continuity of $p(s)$ at the end points of the four different components of the loss function described by Eq. (2.18) (Cox and Isham, 1986; Rodríguez-Iturbe et al., 1999a). In this manner the general solution is obtained as

$$p(s) = \begin{cases} \dfrac{C}{\eta_{\mathrm{w}}} \left(\dfrac{s - s_{\mathrm{h}}}{s_{\mathrm{w}} - s_{\mathrm{h}}} \right)^{\frac{\lambda'(s_{\mathrm{w}} - s_{\mathrm{h}})}{\eta_{\mathrm{w}}} - 1} \mathrm{e}^{-\gamma s} & s_{\mathrm{h}} < s \leq s_{\mathrm{w}} \\ \dfrac{C}{\eta_{\mathrm{w}}} \left[1 + \left(\dfrac{\eta}{\eta_{\mathrm{w}}} - 1 \right) \left(\dfrac{s - s_{\mathrm{w}}}{s^* - s_{\mathrm{w}}} \right) \right]^{\frac{\lambda'(s^* - s_{\mathrm{w}})}{\eta - \eta_{\mathrm{w}}} - 1} \mathrm{e}^{-\gamma s} & s_{\mathrm{w}} < s \leq s^* \\ \dfrac{C}{\eta} \mathrm{e}^{-\gamma s + \frac{\lambda'}{\eta}(s - s^*)} \left(\dfrac{\eta}{\eta_{\mathrm{w}}} \right)^{\lambda' \frac{s^* - s_{\mathrm{w}}}{\eta - \eta_{\mathrm{w}}}} & s^* < s \leq s_{\mathrm{fc}} \\ \dfrac{C}{\eta} \mathrm{e}^{-(\beta + \gamma)s + \beta s_{\mathrm{fc}}} \left(\dfrac{\eta\, \mathrm{e}^{\beta s}}{(\eta - m)\mathrm{e}^{\beta s_{\mathrm{fc}}} + m\, 2\mathrm{e}^{\beta s}} \right)^{\frac{\lambda'}{\beta(\eta - m)} + 1} \left(\dfrac{\eta}{\eta_{\mathrm{w}}} \right)^{\lambda' \frac{s^* - s_{\mathrm{w}}}{\eta - \eta_{\mathrm{w}}}} \mathrm{e}^{\frac{\lambda'}{\eta}(s_{\mathrm{fc}} - s^*)} & s_{\mathrm{fc}} < s \leq 1. \end{cases} \tag{2.39}$$

The expression of the constant C can be obtained analytically, but it is quite involved due to both the piecewise form of the losses and the presence of the

bound (see Appendix A at the end of this chapter). The expressions for the mean and variance of soil moisture are also quite cumbersome and are not reported here. Their behavior was discussed by Rodríguez-Iturbe et al. (1999a) for a simpler model (see Section 2.6.1), but the qualitative behavior is similar to that of the complete model.

Figure 2.8 shows some examples of the pdf's derived from Eq. (2.39). The two different types of soil, already used for Figures 2.6 and 2.7, are loamy sand

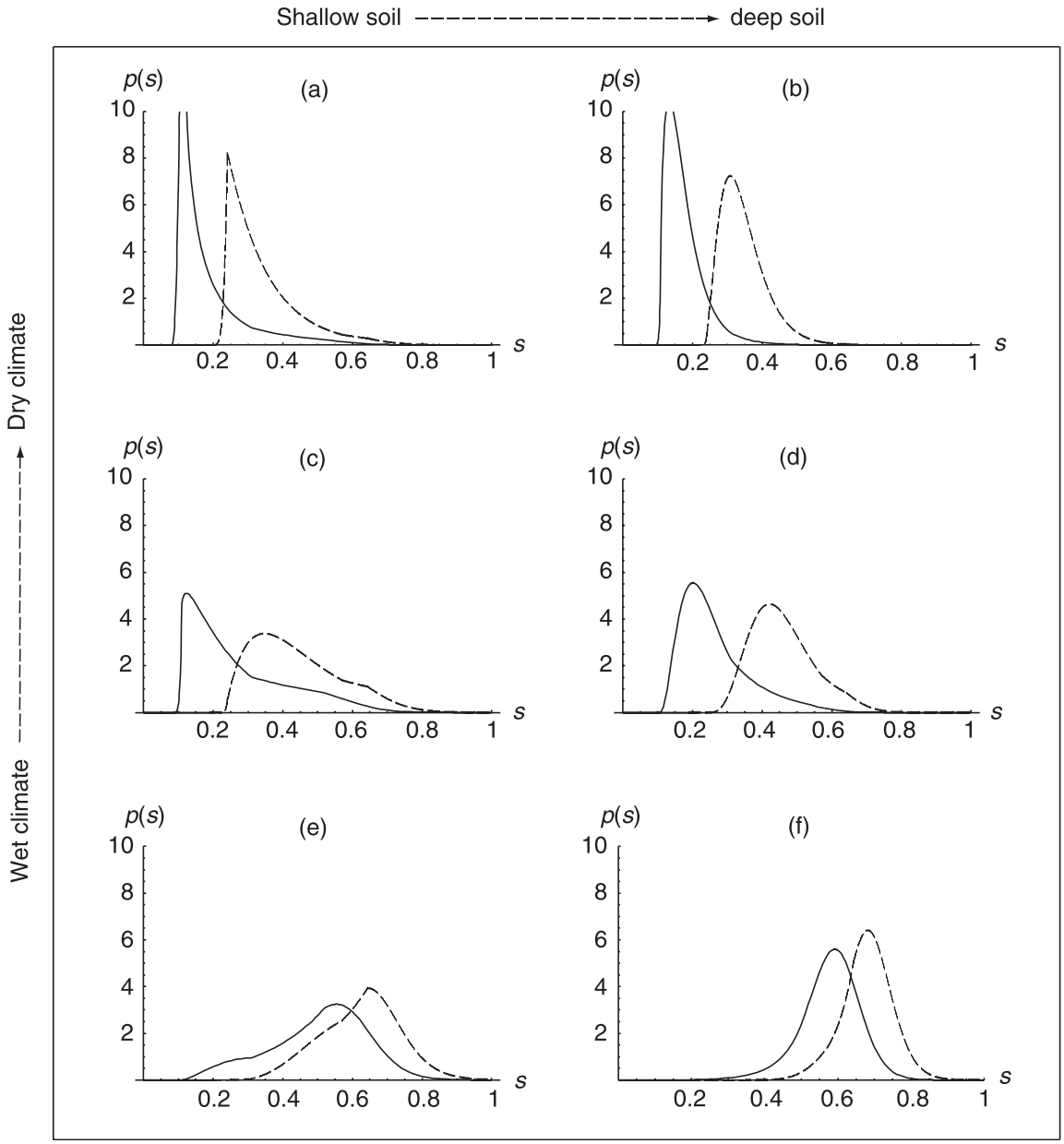

Figure 2.8 Examples of pdf's of relative soil moisture for different type of soil, soil depth, and mean rainfall rate. Continuous lines refer to loamy sand, dashed lines to loam (see Table 2.1 for the values of soil parameters). Left column corresponds to $Z_r = 30\,\text{cm}$, right column to 90 cm. Top, center, and bottom graphs have a frequency of rainfall events λ of 0.1, 0.2, and $0.5\,\text{day}^{-1}$ respectively. Common parameters to all graphs are $\alpha = 1.5\,\text{cm}$, $\Delta = 0\,\text{cm}$, $E_w = 0.01\,\text{cm day}^{-1}$, and $E_{max} = 0.45\,\text{cm day}^{-1}$. After Laio et al. (2001a).

and loam with two different values of active soil depth. These are chosen in order to emphasize the role of soil in the soil moisture dynamics. The parameters related to vegetation are kept fixed and correspond to those used in Table 2.1. A detailed discussion of the role of different functional vegetation types is postponed to the chapters that follow. Here that role of climate is studied only in relation to changes in the frequency of storm events λ, keeping fixed the mean rainfall depth α and the maximum evapotranspiration rate E_{max}. A coarser soil texture corresponds to a consistent shift of the pdf toward drier conditions, which in the most extreme case can reach a difference of 0.2 in the location of the mode. The shape of the pdf also undergoes marked changes, with the broadest pdf's for shallower soils.

Although the qualitative behavior of the pdf's of the earlier model by Rodríguez-Iturbe et al. (1999a) is maintained (see Section 2.6.1), there are important improvements especially in the tails of the distribution. At low levels of soil moisture the residual water content depends directly on the type of soil and vegetation present (see Figure 2.8a in particular). At high soil moisture levels the more realistic representation of leakage provides smoother pdf's for wet conditions and lower values of relative soil moisture as a result of an increased relevance of leakage.

An indication of the impacts of the probabilistic soil moisture dynamics on vegetation is provided by the analysis of particular realizations of soil moisture traces. Figure 2.9 shows a superposition of two traces of soil moisture with the same rainfall realization for the case of a loam with two different active soil

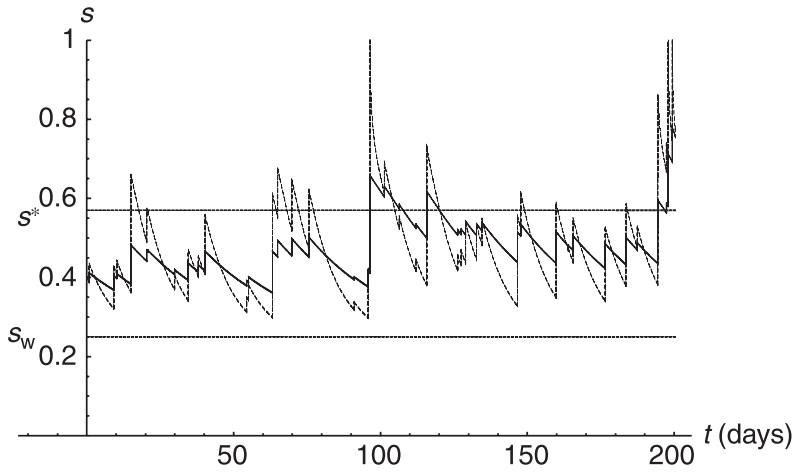

Figure 2.9 Example of traces of relative soil moisture for the same rainfall sequence in a loamy soil with different depths ($\alpha = 1.5$ cm, $\lambda = 0.2$ day^{-1}, $\Delta = 0$ cm, $E_w = 0.01$ cm day^{-1}, $E_{max} = 0.45$ cm day^{-1}; see Table 2.1 for soil parameters). Continuous line refers to $Z_r = 90$ cm, dashed line to $Z_r = 30$ cm. The traces correspond to the pdf's reported with dashed lines in Figures 2.8c and 2.8d. After Laio et al. (2001a).

depths (the parameter values are those used for the dashed line pdf's in Figures 2.8c and 2.8d). In both cases the levels of soil moisture s^* and s_w are the same and so approximately is the mean soil moisture. The continuous line, corresponding to the deeper soil, is almost always between s^* and s_w, which is different from the shallower soil where the trace lively jumps and decays between low and high soil moisture levels. Without anticipating a discussion on vegetation response, the importance of such different soil moisture dynamics for different types of plants and the possible implications for the development of different strategies of adaptation to water stress are nevertheless clearly perceived. A discussion of the impact of climate, soil, and plant water uptake on vegetation response requires a more detailed analysis of the mechanisms of water stress and the definition of quantitative relationships to link such stress to soil moisture dynamics. This will be presented in Chapter 4.

The steady-state analysis is most appropriate for the study of water-controlled ecosystems where rainfall is mostly concentrated in a warm growing season, and winter is usually temperate and dry. As a consequence, in those cases the soil moisture condition at the beginning of the growing season is not very different from that during the rest of the season and transients due to seasonality are generally not significant. Different ecosystems that are examples of these conditions (see Chapter 5) are the savannas of South Africa (Scholes and Walker, 1993), the shrublands in Southern Texas, at least for most of the growing season (Archer et al., 1988; Scholes and Archer, 1997), and the shortgrass steppe in Colorado (Sala et al., 1992). Nevertheless, transient soil moisture dynamics and climatic seasonality can be important in other semi-arid environments, especially at the beginning of the growing season. As will be seen in Chapter 3 and Sections 7.1 and 8.1, this is related to the climatic conditions (e.g., seasonality), to the soil depth, and to the ratio between losses and rainfall input during the months preceding the growing season. Typical cases include Mediterranean climates (e.g., Major, 1963; Naveh, 1967; Ng and Miller, 1980) and the Patagonian steppe (Paruelo and Sala, 1995; Golluscio et al., 1998). Temperate forests in the northwest United States (e.g., Waring and Running, 1998) are also heavily controlled by transient soil moisture conditions. In these cases, rainfall and temperature are markedly out of phase, and the dormant season thus becomes a period of consistent soil-water storage to be used during the following growing season (see Chapter 8).

2.4 Water balance

It is interesting to discuss the soil water balance resulting from the model presented above. The different components of the balance are the long-term

averages of the respective components of the soil moisture dynamics. As described in Eqs. (2.3) through (2.5), rainfall is first partitioned in interception, runoff, and infiltration. The latter is then divided into leakage and evapotranspiration. For the purposes of describing vegetation conditions, the amount of water transpired can be further divided into water transpired under stressed conditions and water transpired under unstressed conditions. This last distinction will be important in relation to the links among soil moisture dynamics, plant water stress, and the structure and productivity of ecosystems.

The long-term average of Eq. (2.3) is simply

$$\langle \varphi \rangle - \langle \chi \rangle = 0. \tag{2.40}$$

Using Eqs. (2.4) and (2.5), the mean infiltration rate is

$$\langle \varphi \rangle = \langle R \rangle - \langle I \rangle - \langle Q \rangle, \tag{2.41}$$

where $\langle R \rangle$, $\langle I \rangle$, and $\langle Q \rangle$ stand for the mean rates of rainfall, interception, and runoff respectively, while the average losses are

$$\langle \chi \rangle = nZ_{\mathrm{r}} \int_{s_{\mathrm{h}}}^{1} \rho(s) p(s)\, \mathrm{d}s. \tag{2.42}$$

The mean rainfall intensity is

$$\langle R \rangle = \alpha \cdot \lambda, \tag{2.43}$$

and the mean rate of interception is (see Section 2.1.2)

$$\langle I \rangle = \alpha \cdot (\lambda - \lambda') = \alpha\lambda\left(1 - \mathrm{e}^{-\frac{\Delta}{\alpha}}\right). \tag{2.44}$$

The water balance Eq. (2.40) can therefore be written as

$$\alpha \cdot \lambda' - \langle Q \rangle = \langle \chi \rangle. \tag{2.45}$$

Returning to the mean rate of water losses from the soil, $\langle \chi \rangle$, this can be also written as

$$\begin{aligned} \langle \chi \rangle = & \langle E_{\mathrm{s}} \rangle + \langle E_{\mathrm{ns}} \rangle + \langle L \rangle = \int_{s_{\mathrm{h}}}^{s^*} E(s)\, p(s)\, \mathrm{d}s \\ & + \int_{s^*}^{1} E(s)\, p(s)\, \mathrm{d}s + \int_{s_{\mathrm{fc}}}^{1} L(s)\, p(s)\, \mathrm{d}s, \end{aligned} \tag{2.46}$$

where $\langle E_{\mathrm{s}} \rangle$, $\langle E_{\mathrm{ns}} \rangle$, and $\langle L \rangle$ are the mean rate of evapotranspiration under stressed conditions, the mean rate of unstressed evapotranspiration, and the mean rate of leakage, respectively.

Analytical expressions for the terms of Eq. (2.46) can be obtained using the simplified forward Eq. (2.33). Integrating Eq. (2.33) from s' to s'', one obtains

$$\int_{s'}^{s''} \rho(s)p(s)\,\mathrm{d}s = \frac{\lambda'}{\gamma}[P(s'') - P(s')] - \frac{1}{\gamma}[\rho(s'')p(s'') - \rho(s')p(s')], \tag{2.47}$$

where $P(s)$ is the cumulative probability distribution of soil moisture (see Appendix A at the end of this chapter). From Eq. (2.47) with $s' = s_h$ and $s'' = s^*$, the analytical expression of $\langle E_s \rangle$ can be calculated as

$$\langle E_s \rangle = \int_{s_h}^{s^*} E(s)p(s)\mathrm{d}s = nZ_r \int_{s_h}^{s^*} \rho(s)p(s)\mathrm{d}s = \alpha\lambda' P(s^*) - \alpha\eta p(s^*), \tag{2.48}$$

where the condition $\eta = \rho(s^*)$ (see Eq. (2.18)) has been used. The evapotranspiration under unstressed conditions can be obtained as

$$\langle E_{ns} \rangle = \int_{s^*}^{1} E(s)p(s)\mathrm{d}s = nZ_r\eta \int_{s^*}^{1} p(s)\mathrm{d}s = E_{max}[1 - P(s^*)], \tag{2.49}$$

and the average leakage losses are

$$\begin{aligned}\langle L \rangle &= \int_{s_{fc}}^{1} L(s)p(s)\mathrm{d}s = nZ_r \int_{s_{fc}}^{1} [\rho(s) - \eta]p(s)\mathrm{d}s \\ &= \alpha\left[\lambda' - \lambda' P(s_{fc}) - \left(\eta + \frac{K_s}{nZ_r}\right)p(1) + \eta p(s_{fc})\right] - E_{max}[1 - P(s_{fc})],\end{aligned} \tag{2.50}$$

where Eq. (2.47) has been used with $s' = s_{fc}$ and $s'' = 1$; again from Eq. (2.18), $\rho(1) = \eta + \frac{K_s}{nZ_r}$ and $\rho(s_{fc}) = \eta$.

The total mean losses from the soil can now be calculated either by applying Eq. (2.47) with $s' = s_h$ and $s'' = 1$ (see Eq. (2.42)), or by summing Eqs. (2.46), (2.48), and (2.49) and simplifying the terms by using Eq. (2.47) with $s' = s^*$ and $s'' = s_{fc}$,

$$\langle \chi \rangle = \alpha\lambda' - \alpha\left(\eta + \frac{K_s}{nZ_r}\right)p(1). \tag{2.51}$$

Finally, Eq. (2.45) and Eq. (2.51) allow one to write the mean runoff as

$$\langle Q \rangle = \alpha\left(\eta + \frac{K_s}{nZ_r}\right)p(1). \tag{2.52}$$

Figure 2.10 presents examples of the behavior of the various components of the water balance normalized by the mean rainfall rate, for some specific

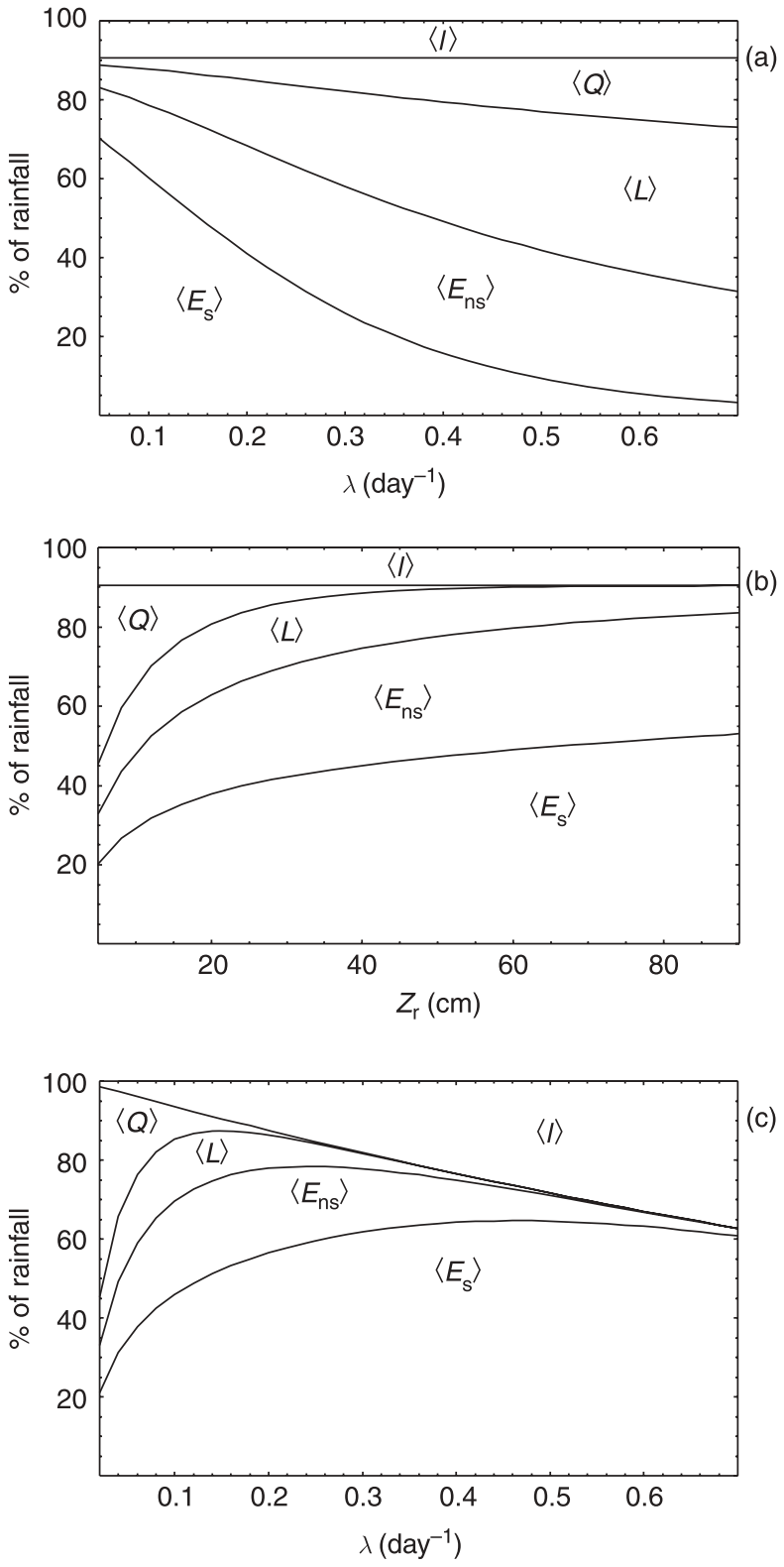

Figure 2.10 Components of the water balance normalized by the total rainfall. (a) Water balance as a function of the frequency of rainfall events λ, for a shallow loamy soil ($Z_r = 30$ cm, $\alpha = 2$ cm). (b) Water balance as a function of the soil depth Z_r, for a loamy sand ($\alpha = 2$ cm, $\lambda = 0.2$ day^{-1}). (c) Water balance for a loamy sand as a function of the frequency of rainfall events for a constant mean total rainfall during a growing season, $\Theta = 60$ cm. Other common parameters are $E_w = 0.01$ cm day^{-1}, $E_{max} = 0.45$ cm day^{-1}, and $\Delta = 0.2$ cm (see Table 2.1 for soil parameters). After Laio et al. (2001a).

rainfall, soil, and vegetation characteristics. The influence of the frequency of rainfall events, λ, is shown in Figure 2.10a for the case of a shallow loam. Since the amount of interception changes in proportion to the rainfall rate, it is not surprising that the fraction of water intercepted remains constant when normalized by the total rainfall, $\alpha\lambda$. The percentage of runoff increases almost linearly. More interesting is the interplay between leakage and the two components of evapotranspiration. The fraction of water transpired under stressed conditions rapidly decreases from $\lambda = 0.1$ to about $\lambda = 0.4$, while the evapotranspiration under unstressed conditions evolves in a much more gentle manner. As will be discussed in Chapter 4, this last aspect has interesting implications for vegetation productivity. It is clear that in semi-arid conditions most of the water that actually reaches the soil is lost by evapotranspiration (in particular transpiration), a result in agreement with many field observations (e.g., Sarmiento, 1984; Eagleson and Segarra, 1985; Sala et al., 1992; Scholes and Walker, 1993).

Figure 2.10b shows the role of the active soil depth in the water balance. For relatively shallow soils there is a strongly nonlinear dependence on soil depth of all components of the water balance (with the obvious exception of interception, which is constant because the rainfall is constant). For example, changing from $nZ_r = 5$ to $nZ_r = 20$ the amount of water transpired is practically doubled in this particular case.

Figure 2.10c shows the impact on water balance when the frequency and amount of rainfall are varied keeping constant the total amount of rainfall in a growing season. The result is interesting, because of the existence of two opposite mechanisms regulating the water balance. On one hand, runoff production, for a given mean rainfall input, strongly depends on the ratio between soil depth and the mean depth of rainfall events. The rapid decrease of runoff is thus somewhat analogous to that in the first part of Figure 2.10b, where a similar behavior was produced by an increase in soil depth. On the other hand interception increases almost linearly with λ. The interplay between these two mechanisms determines a maximum of both leakage and evapotranspiration at moderate values of λ (of course the position of the maxima changes according to the parameters used). This is particularly important from the vegetation point of view, since the mean transpiration rate is linked to productivity of ecosystems (e.g., Kramer and Boyer, 1995, page 383). The role not only of the amount, but also of the timing of rainfall in soil moisture dynamics (Noy-Meir, 1973), is made clear by the existence of an optimum for transpiration/productivity, which is directly related to the climate–soil–vegetation characteristics. The particular position of this maximum in the parameter space is governed by the interplay of all the mechanisms acting

in the soil water balance; namely, the intensity and amount of rainfall, interception, the active soil depth, and the nonlinear losses due to evapotranspiration and leakage.

2.5 Comparison with field data

The analytical solution of the stochastic model of soil water balance is illuminating in many issues, because it allows a quantitative comprehensive view of the soil moisture dynamics and related phenomena. The results are in good agreement with physical expectations. Other investigations on soil moisture dynamics have used similar assumptions, concerning both the stochastic representation of rainfall (e.g., Eagleson, 1978a, 1978b; Cordova and Bras, 1981; Milly, 1993) and the behavior of losses due to evapotranspiration and leakage (e.g., Cordova and Bras, 1981; Paruelo and Sala, 1995). Here we discuss some recent field data that provide further support for the model assumptions. More detailed comparisons with natural ecosystems of different types will be given in Chapter 5.

The first set of information concerns the three-stage sequence of evapotranspiration losses from a shortgrass steppe, analyzed by Brutsaert and Chen (1995, 1996). Using data sampled at a daily time scale, which is also the time scale adopted here, they reported the existence of three phases of drying with distinct temporal behavior. Such phases could correspond to the three different types of soil moisture control of evapotranspiration of the present model (e.g., Eq. (2.14)). According to their analysis, during the first stage of drying after an abundant rainfall, soil water evaporates from both the soil surface and vegetation, at a rate that is governed by the available energy supply. This phase corresponds in our model to the range of soil moisture $\{s^*, 1\}$ or, according to Eq. (2.22), to the time interval $0 < t \leq t_{s^*}$. Then, after soil moisture content has decreased below a critical level, a transitional stage sets in, during which soil moisture is the controlling factor. This agrees with the assumptions of the model presented in this chapter, where soil moisture controls transpiration through stomatal closure between s_w and s^*, or in the interval $t_{s^*} < t \leq t_{s_w}$. Finally, when soil moisture decreases below a certain threshold corresponding to plant wilting, drying takes place mainly as evaporation from the soil surface ($s_h < s \leq s_w$, or $t_{s_w} < t \leq \infty$). Brutsaert and Chen (1995) refer to this phase as a desorption phase with a temporal decay proportional to $t^{-0.5}$, but they also maintain that different mathematical formulations could be possible for this phase. Moreover, the relevance of this last phase for modeling purposes is limited, except for extremely dry environments.

Some important field support for the theoretical results presented before comes from the recent analysis by Salvucci (2001). By noticing that the expected value of the change in soil moisture storage, conditioned on the storage s, is zero under statistically steady-state conditions, he deduced that the conditionally averaged net precipitation rate is equal to the moisture-dependent losses. Thus, using daily precipitation and average soil moisture data from a site in Illinois, and dividing the sample into two parts, one corresponding to the early growing season and the other to the late growing season, Salvucci (2001) estimated the conditionally averaged precipitation rate for various values of soil moisture. In this manner, from field data, he then obtained soil moisture daily losses whose functional form closely agrees with the one used here, namely Eq. (2.18). Figure 2.11a reproduces the loss functions obtained by Salvucci (2001). Employing these loss functions, jointly with the estimates of the frequency of occurrence and mean depth of daily rainfall, λ and α, Salvucci (2001) also computed the relative soil moisture pdf's with Eq. (2.37), obtaining an excellent match with the observed frequency distributions (Figure 2.11b).

2.6 Simpler models of soil moisture dynamics

The loss function previously used (see Eq. (2.18) and Figure 2.5) attempts a balance between a realistic representation of the processes involved and mathematical tractability. In some cases, however, when the main focus is not on the soil moisture–vegetation interaction, the loss function may be further simplified and still provide a useful description of the processes that are at the basis of the water balance. Three different types of loss functions with increasing level of simplification are considered in this section: the simplified model studied by Rodríguez-Iturbe et al. (1999a), the minimalistic model proposed by Milly (1993, 2001), and a simple alternative to the latter.

2.6.1 A simplified stochastic model of soil moisture dynamics

The model proposed by Rodríguez-Iturbe et al. (1999a) is an earlier version of the more complete model presented in this chapter. Although somewhat less suitable for ecohydrological studies, it still retains important features and is worth considering because of its simpler expressions for both the mean soil moisture and the water balance components.

The precipitation and infiltration models are the same as in Sections 2.1.1 through 2.1.4. The only part that differs from the previously described model is the loss function, namely the evapotranspiration at very low values of soil

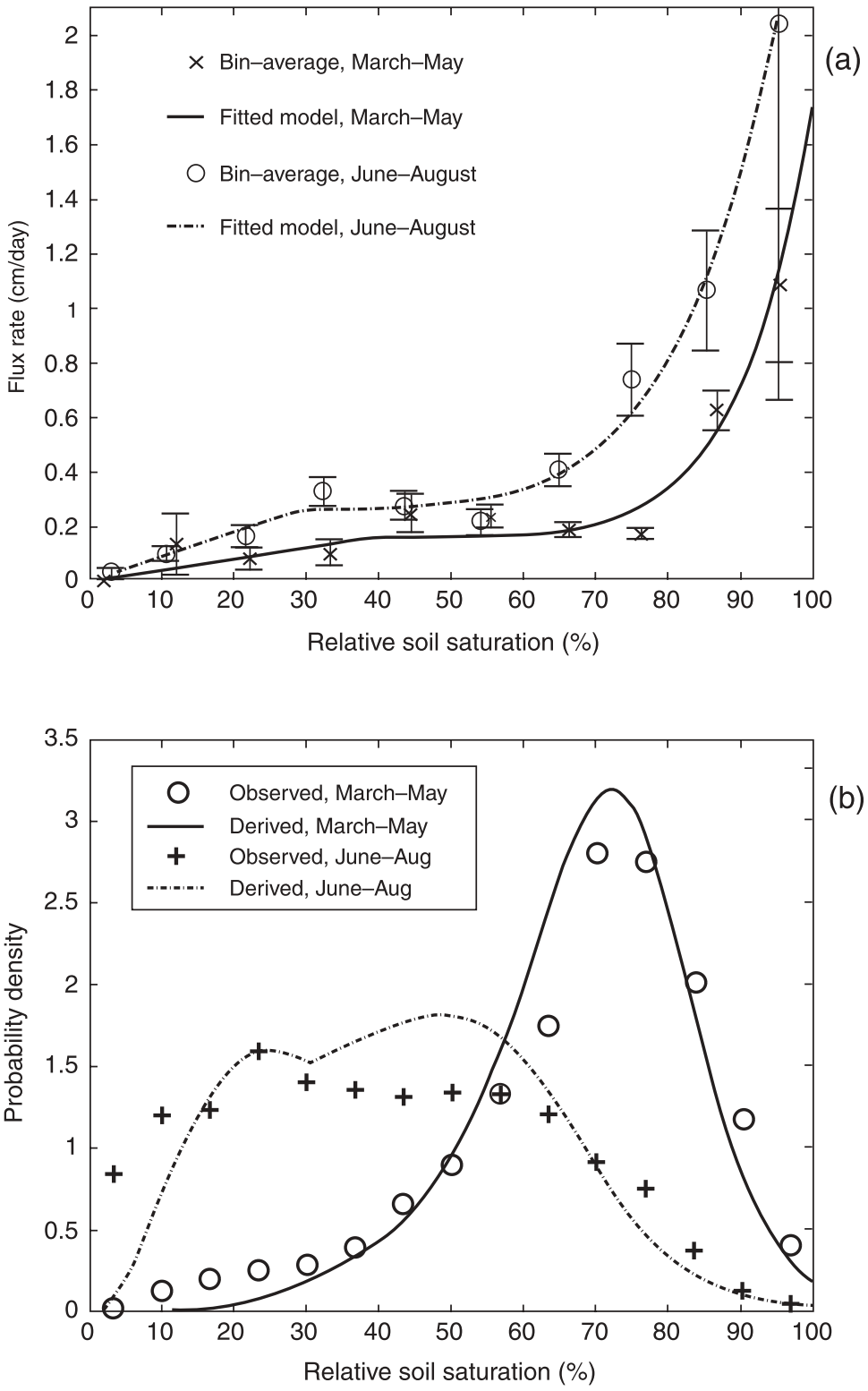

Figure 2.11 (a) Estimation of water loss from conditional mean precipitation for a site in Illinois. (b) Observed and derived probability distributions of relative soil saturation (after Salvucci, 2001).

moisture and the leakage. Evapotranspiration is assumed to increase linearly from 0 at $s = 0$ to E_{max} at s^* and then remain constant until saturation. Leakage is simply a linearly increasing function from 0 at a given threshold $s_1 > s_{fc}$ up to K_s at saturation.

Because of the form of the losses, the pdf is now

$$p(s) = \begin{cases} \frac{C'}{\eta}\left(\frac{s}{s^*}\right)^{\frac{\lambda s^*}{\eta}-1} \mathrm{e}^{-\gamma s} & 0 < s \le s^* \\ \frac{C'}{\eta}\ \mathrm{e}^{-\frac{\lambda s^*}{\eta}}\ \mathrm{e}^{-s\left(\gamma-\frac{\lambda}{\eta}\right)} & s^* < s \le s_1 \\ \frac{C'}{\eta}\left[\frac{k(s-s_1)}{(1-s_1)\eta}+1\right]^{\frac{\lambda(1-s_1)}{k}-1} \mathrm{e}^{-\gamma s+\lambda\frac{s_1-s^*}{\eta}} & s_1 < s \le 1. \end{cases} \tag{2.53}$$

The expression for C' resulting from the normalizing condition, Eq. (2.38), is

$$C' = \frac{\eta\ \zeta\ k\ \mathrm{e}^{\chi}\ R}{\eta\zeta k(\mathrm{e}^{\chi-\gamma s^*} - \mathrm{e}^{\lambda s_1/\eta+\gamma s^*}) + \eta\zeta\xi\,\mathrm{e}^{\vartheta}(1-s_1)R(\Gamma_2-\Gamma_1) + \mathrm{e}^{\chi}ks^*R\Gamma_3}, \tag{2.54}$$

where

$$\begin{aligned} R &= \gamma\eta - \lambda \\ \zeta &= (\gamma s^*)^{\frac{\lambda s^*}{\eta}} \\ \vartheta &= \frac{\gamma\eta(1-s_1)}{k} + \frac{\lambda s_1}{\eta} + \gamma s^* \\ \xi &= \left[\frac{\gamma\eta(1-s_1)}{k}\right]^{\frac{-\lambda(1-s_1)}{k}} \\ \chi &= \gamma(s_1+s^*) + \frac{\lambda s^*}{\eta} \\ \Gamma_1 &= \Gamma[\lambda(1-s_1)/k, \gamma\eta(1-s_1)/k] \\ \Gamma_2 &= \Gamma[\lambda(1-s_1)/k, \gamma(\eta+k)(1-s_1)/k] \\ \Gamma_3 &= \Gamma[\lambda s^*/\eta, \gamma s^*] \end{aligned} \tag{2.55}$$

and $\Gamma(\cdot,\cdot)$ stands for the generalized incomplete gamma function.

The expression for the mean, $\langle s\rangle = \int_0^1 s\ p(s)\,\mathrm{d}s$, can be obtained as

$$\begin{aligned} \langle s\rangle = c\Bigg\{ &\left[\varphi_1 \mathrm{e}^{-\gamma s_1+\frac{\lambda}{\eta}(s_1-s^*)+\gamma s^*} - \varphi_2 \mathrm{e}^{-\gamma s^*}\right] \\ &+\xi \mathrm{e}^{\vartheta-\chi}\frac{1-s_1}{k}\left[(\Gamma_1-\Gamma_2)\frac{\eta(1-s_1)-ks_1}{k} - \frac{1}{\gamma}(\Gamma_4-\Gamma_5)\right] + \frac{s^*}{\zeta\eta\gamma}\Gamma_6\Bigg\}, \end{aligned} \tag{2.56}$$

where the new symbols are defined as

$$\varphi_1 = \frac{-\eta - s_1(\gamma\eta - \lambda)}{(\gamma\eta - \lambda)^2}$$

$$\varphi_2 = \frac{-\eta - s^*(\gamma\eta - \lambda)}{(\gamma\eta - \lambda)^2}$$

$$\Gamma_4 = \Gamma[1 + \lambda(1 - s_1)/k, \gamma\eta(1 - s_1)/k]$$

$$\Gamma_5 = \Gamma[\ 1 + \lambda(1 - s_1)/k, \gamma(\eta + k)(1 - s_1)/k]$$

$$\Gamma_6 = \Gamma[1 + \lambda s^*/\eta, \gamma s^*]. \tag{2.57}$$

Notice that Γ_4, Γ_5, and Γ_6 are related to Γ_1, Γ_2, and Γ_3 respectively (e.g., Abramowitz and Stegun, 1964), but this does not allow for further simplifications. The variance may also be obtained analytically but it is a long expression that adds little by itself.

Figure 2.12 shows the impact of evapotranspiration, rate of storm arrivals, and mean depth per event on the mean soil moisture. The soil characteristics

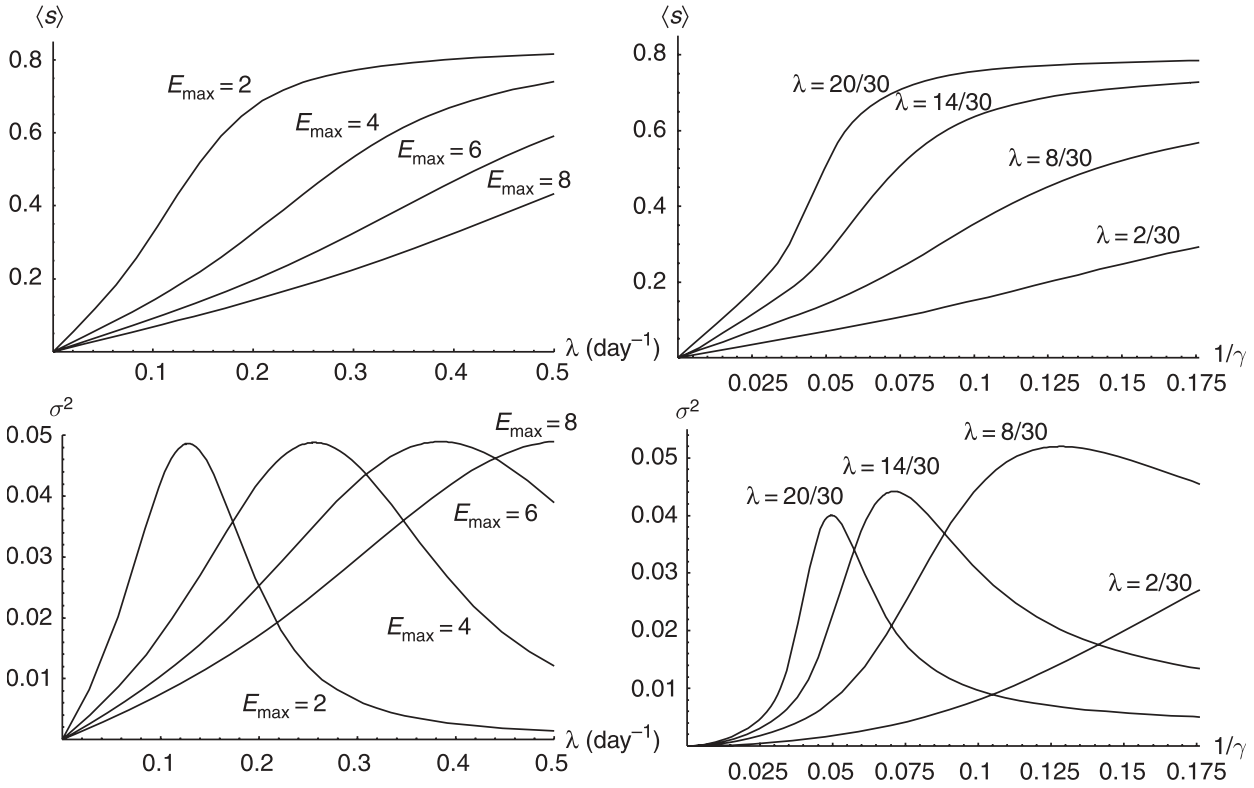

Figure 2.12 Mean and variance of soil moisture as a function of rainfall and evapotranspiration parameters ($s^* = 0.35$, $s_1 = 0.85$, $K_s = 100\,\text{cm day}^{-1}$, $nZ_r = 15\,\text{cm}$). Left column: $1/\gamma = 15/1.5$; right column: $E_{max} = 5\,\text{mm day}^{-1}$. Redrawn after Rodriguez-Iturbe et al. (1999a).

are taken in the middle range of their possible values. Notice how, when rain events occur very frequently, the mean value of the soil moisture becomes highly dependent on the mean storm depth up to a point after which it remains practically constant and close to saturation.

The variance of the soil moisture pdf is also shown in Figure 2.12 for a fixed set of soil conditions as a function of the characteristics of rainfall and evapotranspiration. One can observe the high sensitivity of the variance to rainfall and evapotranspiration rates. Except for very dry climates, the soil moisture variance has a well-defined maximum. Thus for a given mean frequency of rain events, the variance increases with increasing active soil depth up to a point after which any further increase in soil depth leads to a decrease in variance. The point at which the maximum occurs varies with the frequency of events and is also a function of the soil and vegetation parameters.

Rodríguez-Iturbe et al. (1999a) also give the expressions of the normalized components of the average water balance, which can be expressed in a simpler form than those of the full model (Section 2.4). As for the mean and variance, due to the averaging operation, the differences with the full model are even smaller.

2.6.2 *Minimalistic models of soil moisture dynamics*

In the minimalistic model proposed by Milly (1993, 2001) the losses are assumed to be constant and equal to $E_{\max}$ in the range $s_w < s < s_1$ and zero at s_w. Above s_1, leakage and runoff losses take place instantaneously (i.e., at an infinite rate, $K_s \to \infty$), so that s_1 is the effective upper bound of the process. Although Milly's model may be too simplified for a meaningful description of plant conditions, its parsimony in the number of parameters makes it interesting as a theoretical simplified description of the mean water balance. From a mathematical viewpoint Milly's model corresponds to the virtual waiting-time process with the addition of an upper bound at s_1. Such a process has been a well-studied one since Takacs pointed out its importance in the queuing and storage context, where the state variable is interpreted as the total time it would take to serve all customers in an office at time t, or the time-dependent amount of water in a reservoir depleted at a constant rate (e.g., Cox and Miller, 1965, page 241).

Since in this model the soil moisture fluctuates only between s_w and s_1, one can introduce a new variable

$$x = \frac{s - s_w}{s_1 - s_w}, \tag{2.58}$$

which will be called effective relative soil moisture, and define the available water storage as $w_0 = (s_1 - s_w)nZ_r$. In the new variable x, the only relevant parameters are w_0, λ, α, and E_{max}. Using dimensional analysis, the problem can be expressed as a function of only two dimensionless variables. Possible choices (Milly, 2001) are either

$$\gamma = \frac{w_0}{\alpha} \quad \text{and} \quad \frac{\lambda}{\eta} = \frac{\lambda w_0}{E_{max}}, \tag{2.59}$$

which are similar to those used before, or

$$\gamma = \frac{w_0}{\alpha} \quad \text{and} \quad D_I = \frac{\gamma\eta}{\lambda} = \frac{E_{max}}{\langle R \rangle}, \tag{2.60}$$

where D_I is the dryness index of Budyko (1974), which represents the long-term ratio between the potential evapotranspiration and the rainfall rate.

Since in this case the losses approach s_w (i.e., $x = 0$) discontinuously, the soil moisture pdf is a mixed distribution with an atom of probability at $x = 0$. The normalized form of Eqs. (2.29) and (2.30) becomes

$$\frac{\partial}{\partial\tau}p(x,\tau) = \frac{\eta}{\lambda}\frac{\partial}{\partial x}p(x,\tau) - p(x,\tau) + \gamma\int_0^x p(u,\tau)\,\mathrm{e}^{-\gamma(x-u)}\,\mathrm{d}u + \gamma\,p_0(\tau)\,\mathrm{e}^{-\gamma x}, \tag{2.61}$$

$$\frac{\mathrm{d}}{\mathrm{d}\tau}p_0(\tau) = -p_0(\tau) + \frac{\eta}{\lambda}\,p(0,\tau), \tag{2.62}$$

where $\tau = \lambda t$. The steady-state solution can be obtained as

$$p(x) = \frac{\lambda}{\eta}\;p_0\,\mathrm{e}^{\left(\frac{\lambda}{\eta}-\gamma\right)x}, \tag{2.63}$$

$$p_0 = \frac{\frac{\lambda}{\eta} - \gamma}{\frac{\lambda}{\eta}\;\mathrm{e}^{\frac{\lambda}{\eta}-\gamma} - \gamma}. \tag{2.64}$$

In the special case when $\frac{\lambda}{\eta} = \gamma$ (e.g., $D_I = 1$),

$$p(x) = \frac{\gamma}{1+\gamma}, \quad p_0 = \frac{1}{1+\gamma}. \tag{2.65}$$

The continuous part of the steady-state pdf is thus an exponential function (see Figures 2.13 and 2.14a) which becomes uniform for $\frac{\lambda}{\eta} = \gamma$ (e.g., $D_I = 1$).

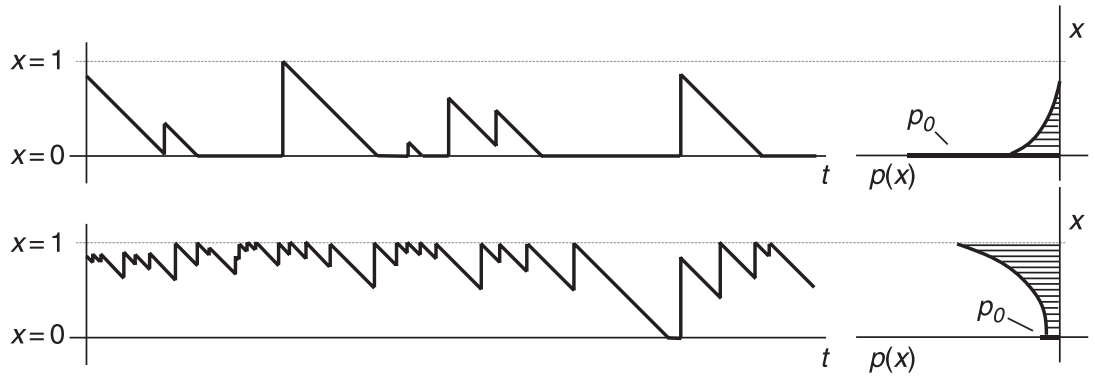

Figure 2.13 Examples of traces and steady-state pdf's for Milly's model.

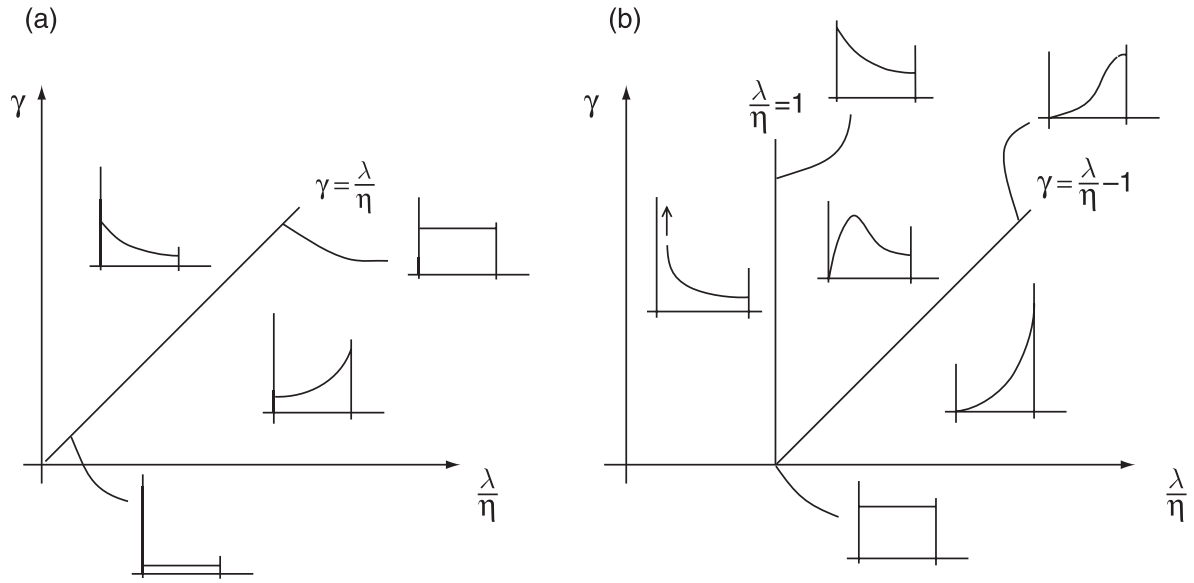

Figure 2.14 Different forms of the relative soil moisture steady-state pdf's for (a) the minimalistic model with constant losses and (b) with linearly increasing losses with soil moisture.

Although the resulting pdf's of these minimalistic models are too coarse a description of the soil moisture process, both the mean and variance as well as the mean components of the water balance show some resemblance to those of the full model described before (see Milly, 2001). The mean and variance are given by

$$\langle x \rangle = \frac{1}{\frac{\lambda}{\eta} - \gamma} + \frac{1 + \frac{\lambda}{\eta}\, e^{\frac{\lambda}{\eta} - \gamma}}{\frac{\lambda}{\eta}\, e^{\frac{\lambda}{\eta} - \gamma} - \gamma}, \tag{2.66}$$

$$\sigma_x^2 = \frac{1}{\left(\frac{\lambda}{\eta} - \gamma\right)^2} - \frac{1 + (\gamma + 2)\frac{\lambda}{\eta}\, e^{\frac{\lambda}{\eta} - \gamma}}{\left(\frac{\lambda}{\eta}\, e^{\frac{\lambda}{\eta} - \gamma} - \gamma\right)^2}. \tag{2.67}$$

In the special case $\frac{\lambda}{\eta} = \gamma$ (e.g., $D_I = 1$), the limit yields

$$\langle x \rangle = \frac{\gamma}{2(1+\gamma)}, \quad \sigma_x^2 = \frac{\gamma^2 + 4\gamma}{12(\gamma+1)^2}. \tag{2.68}$$

Neglecting interception (e.g., $\lambda = \lambda'$, $\Delta = 0$), the water balance is simply given by the partition between long-term evapotranspiration $\langle E \rangle$ and leakage plus runoff $\langle LQ \rangle$, i.e.,

$$\langle R \rangle = \langle E \rangle + \langle LQ \rangle = E_{\max}(1 - p_0) + \langle LQ \rangle. \tag{2.69}$$

Normalizing with the mean total rainfall and introducing the dryness index, one readily obtains

$$\frac{\langle E \rangle}{\langle R \rangle} = D_I\,(1 - p_0), \tag{2.70}$$

$$\frac{\langle LQ \rangle}{\langle R \rangle} = 1 - D_I\,(1 - p_0), \tag{2.71}$$

where p_0 is given by Eqs. (2.64) and (2.65).

An alternative minimalistic model is obtained by assuming linear increasing evapotranspiration losses with soil moisture (Porporato et al., 2004). In this case soil moisture decays exponentially, so that x approaches zero only asymptotically. As a consequence, the corresponding steady-state pdf has no atom at zero and reads

$$p(x) = \frac{C''}{\eta}\, \mathrm{e}^{-\gamma x} x^{\frac{\lambda}{\eta}-1}, \tag{2.72}$$

where

$$C'' = \frac{\eta\, \gamma^{\frac{\lambda}{\eta}}}{\Gamma\left(\frac{\lambda}{\eta}\right) - \Gamma\left(\frac{\lambda}{\eta}, \gamma\right)}. \tag{2.73}$$

As shown in Figure 2.14, the pdf of this new minimalistic model shows a richer behavior than the corresponding model with constant losses.

The mean is given by

$$\langle x \rangle = \frac{\lambda}{\gamma\,\eta} - \frac{\gamma^{\frac{\lambda}{\eta}-1}\, \mathrm{e}^{-\gamma}}{\Gamma\left(\frac{\lambda}{\eta}\right) - \Gamma\left(\frac{\lambda}{\eta}, \gamma\right)}, \tag{2.74}$$

and the normalized water balance is easily obtained by noticing that $\langle E \rangle = E_{\max} \langle x \rangle$. Hence

$$1 = D_I \langle x \rangle + \frac{\langle LQ \rangle}{\langle R \rangle}. \tag{2.75}$$

Figure 2.15 shows a computation of the fraction of evapotranspiration losses for the two minimalistic models described above. Interestingly, the results reproduce qualitatively analogous empirical curves that have been used to describe observational data for the mean annual water balance over large regions (e.g., Budyko, 1974; Brutsaert, 1982) and, in particular, the well-known hydroclimatological relationship of Budyko (1974). The latter describes the average terrestrial water balance by means of a semi-empirical curve which represents the fraction of the rainfall that is evapotranspired as a nonlinear function of the dryness index,

$$\langle E/R \rangle = \{D_I[1 - \exp(-D_I)] \tanh(1/D_I)\}^{0.5}, \tag{2.76}$$

and synthesizes the average partitioning of the rainfall input into evapotranspiration and runoff plus deep infiltration, thus offering a parsimonious and universal picture of the terrestrial water cycle. As shown in detail in Figure 2.16, for $\gamma \sim 5.5$ the minimalistic model with linear losses reproduces very well Budyko's curve. Therefore, using typical values of the parameters (e.g., average rainfall depth per event $\alpha = 1.5$ cm, relative soil moisture at the wilting point $s_w = 0.2$, relative soil moisture threshold for deep infiltration and runoff

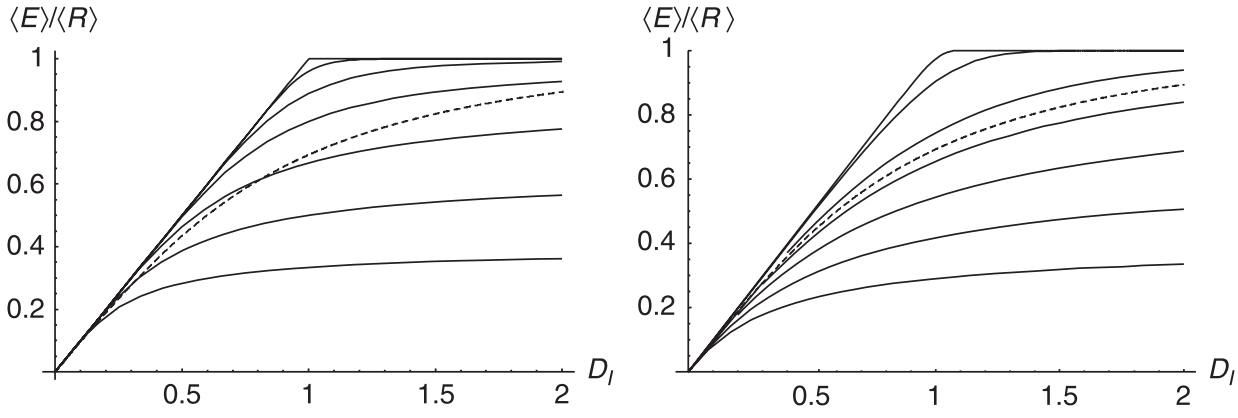

Figure 2.15 Comparison of the two minimalistic models. Fraction of precipitation that is evapotranspired as a function of the dryness index for various values of the dimensionless soil water-holding capacity, γ. Values of γ are from bottom to top: 0.5, 1, 2, 4, 8, 24, and 1000. Dashed line: Budyko's curve, Eq. (2.76). Left: minimalistic model with constant losses (modified after Milly, 1993); right: minimalistic model with losses linearly increasing with soil moisture.

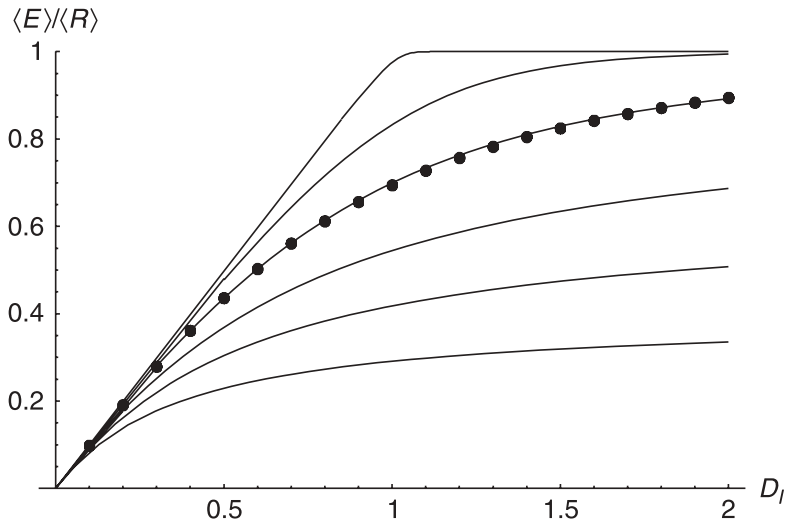

Figure 2.16 Fraction of total rainfall lost by evapotranspiration as a function of Budyko's dryness index for different values of the parameter γ for the minimalistic model with linear losses. The dots represent the semi-empirical curve of Budyko, while the continuous line underlying the dots corresponds to $\gamma = 5.5$. As explained in the text, this refers to an average effective rooting depth of approximately 35 cm. From the lowest to the highest one, the continuous curves refer to $\gamma = 0.5$, 1, 2, 5.5, 20, 1000, respectively. After Porporato et al. (2004).

$s_1 = 0.85$, and porosity $n = 0.4$), Budyko's curve corresponds to an average active soil depth of approximately 30–35 cm which, interestingly, is the average depth within which most of the roots are typically comprised (Jackson et al., 1996; Schenk and Jackson, 2002). The model interpretation also makes clear the effects of possible climate changes on Budyko's curve. As an example, depending on the degree to which evapotranspiration, rainfall regime and plant characteristics are affected by climate change, alterations in the mean depth of rainfall per event and in the rooting depth will imply a vertical shift in the diagram, while a shift along the x-axis will entail changes in potential transpiration and total amounts of rainfall (Porporato et al., 2004).

Thanks to the realistic representation of the soil water balance provided by the minimalistic model with linear losses, the corresponding behavior of the pdf of the effective relative soil moisture as a function of the governing parameters may be used for a general classification of soil moisture regimes. Accordingly, the boundaries between different shapes of the pdf may be used to define an "arid" regime (pdf's with zero mode), an "intermediate" regime (corresponding to soil moisture pdf's with a central maximum) and a "wet" regime (with the mode at saturation) as indicated in Figure 2.17. A further distinction within the intermediate regime can be made on the basis of plant response to soil moisture dynamics. Using the effective relative soil moisture value (x^*) as a threshold marking the onset of plant water stress (as will be seen

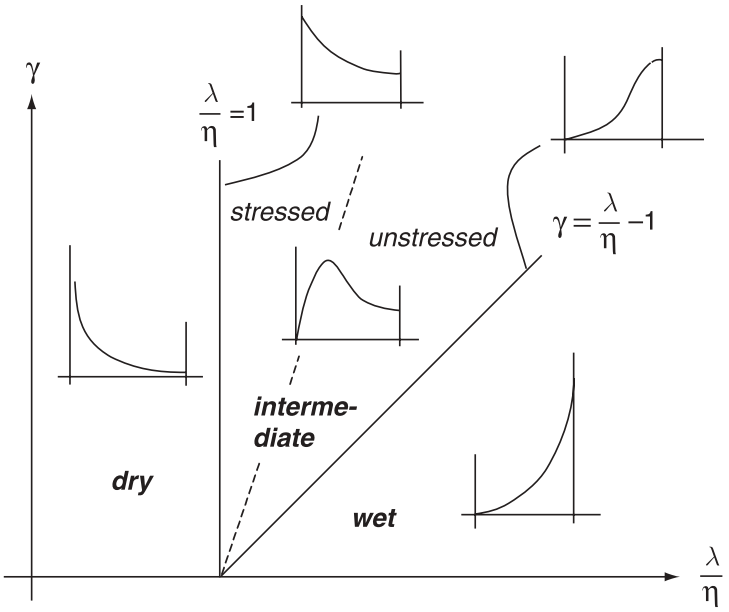

Figure 2.17 Classification of soil water balance, based on the shape of the effective relative soil moisture pdf, as a function of the two governing parameters, λ/η and γ, that synthesize the role of climate, soil, and vegetation. The dashed line, $\gamma = 1/x^*(\lambda/\eta - 1)$, is the locus of points where the mode of the soil moisture pdf is equal to the threshold x^*, which marks the onset of plant water stress. After Porporato et al. (2004).

in Chapter 4, x^* is typically in the order of 0.3–0.4), the dashed line of slope $1/x^*$ in Figure 2.17 becomes the place where the mode of the effective relative soil moisture pdf is equal to x^* and thus where plants are more likely to be at the boundary between stressed and unstressed conditions. Accordingly, it may be used to divide water-stressed (or semi-arid) types of water balance on the left side from unstressed ones on the right side (Figure 2.17).

2.7 Appendix A. Soil moisture cumulative probability distribution

The analytical expressions of the cumulative probability distribution $P(s)$ of soil moisture are reported here, using the parameters defined in Eqs. (2.19), (2.20), and (2.21). The expression is split into four parts resulting from the piecewise loss function Eq. (2.18). The expression for $P(s)$ is obtained by direct integration of the pdf of soil moisture given by Eq. (2.39).

For $s_h < s \leq s_w$ the cumulative distribution is

$$P(s) = \frac{C}{\eta_w} e^{-\gamma s_h} (s_w - s_h)[\gamma(s_w - s_h)]^{-\frac{\lambda'(s_w - s_h)}{\eta_w}} \left\{ \Gamma\left[\frac{\lambda'(s_w - s_h)}{\eta_w}\right] + \Gamma\left[\frac{\lambda'(s_w - s_h)}{\eta_w}, \gamma(s - s_h)\right] \right\}, \tag{2.77}$$

where $\Gamma[\,\cdot\,]$ and $\Gamma[\,\cdot\,,\,\cdot\,]$ are the complete and incomplete gamma function, respectively (Abramowitz and Stegun, 1964, n. 6.1.1 and n. 6.5.3). For $s_w < s \leq s^*$ the expression for $P(s)$ takes the form

$$P(s) = P(s_w) + \frac{C}{\eta - \eta_w}(s^* - s_w)\left[\frac{\eta_w \gamma(s^* - s_w)}{\eta - \eta_w}\right]^{-\lambda' \frac{s^* - s_w}{\eta - \eta_w}} e^{-\gamma\left[s_w - \frac{\eta_w(s^* - s_w)}{\eta - \eta_w}\right]}$$
$$\times \left\{\Gamma\left[\lambda' \frac{s^* - s_w}{\eta - \eta_w}, \frac{\eta_w \gamma(s^* - s_w)}{\eta - \eta_w}\right]\right.$$
$$\left. + \Gamma\left[\lambda' \frac{s^* - s_w}{\eta - \eta_w}, \gamma(s - s_w) + \frac{\eta_w \gamma(s^* - s_w)}{\eta - \eta_w}\right]\right\}, \tag{2.78}$$

where $P(s_w)$ is the value of the cumulative probability distribution calculated in $s = s_w$ from Eq. (2.77). When $s_w < s \leq s^*$ the cumulative probability distribution is

$$P(s) = P(s^*) + \frac{C}{\lambda' - \gamma\eta}\left(\frac{\eta}{\eta_w}\right)^{\lambda' \frac{s^* - s_w}{\eta - \eta_w}}\left[e^{-\gamma s + \frac{\lambda'}{\eta}(s - s^*)} - e^{-\gamma s^*}\right], \tag{2.79}$$

with the value of $P(s^*)$ calculated from Eq. (2.78). Finally, for $s_{fc} < s \leq 1$ the expression for $P(s)$ can be written as

$$P(s) = P(s_{fc}) + \frac{C}{\gamma(\eta - m) - \lambda'}\left(\frac{\eta}{\eta_w}\right)^{\lambda' \frac{s^* - s_w}{\eta - \eta_w}} e^{\frac{\lambda'}{\eta}(s_{fc} - s^*)}\left\{e^{-\gamma s_{fc}}\left(\frac{\eta}{\eta - m}\right)^{\frac{\lambda'}{\beta(\eta - m)}}\right.$$
$$\times {}_2F_1\left[\frac{\lambda'}{\beta(\eta - m)} + 1, \frac{\lambda'}{\beta(\eta - m)} - \frac{\gamma}{\beta}; \frac{\lambda'}{\beta(\eta - m)} + 1 - \frac{\gamma}{\beta}; \frac{m}{m - \eta}\right]$$
$$- e^{-\gamma s}\left[\frac{\eta}{\eta - m} \cdot \frac{e^{\beta(s - s_{fc})} m + \eta - m}{e^{-\beta(s - s_{fc})}(\eta - m) + m}\right]^{\frac{\lambda'}{\beta(\eta - m)}}$$
$$\left. \times {}_2F_1\left[\frac{\lambda'}{\beta(\eta - m)} + 1, \frac{\lambda'}{\beta(\eta - m)} - \frac{\gamma}{\beta}; \frac{\lambda'}{\beta(\eta - m)} + 1 - \frac{\gamma}{\beta}; \frac{e^{\beta(s - s_{fc})} m}{m - \eta}\right]\right\}, \tag{2.80}$$

where $P(s_{fc})$ is calculated from Eq. (2.79) and ${}_2F_1[\,\cdot\,,\,\cdot\,;\,\cdot\,;\,\cdot\,]$ is the Hypergeometric Function (Abramowitz and Stegun, 1964, n. 15.1.1).

The integration constant C in Eqs. (2.77)–(2.80) is the same of Eq. (2.39). The analytical expression of C can be derived by imposing the condition $P(1) = 1$ in Eq. (2.80), and noting that $P(s_{fc})$ in Eq. (2.80) is a function of C as well.